Conjugated Polymer Polypyrrole Nanostructures: Synthesis and Photocatalytic Applications

Xiaojiao Yuan, Hynd Remita

Conjugated Polymer Polypyrrole Nanostructures: Synthesis and Photocatalytic Applications

Xiaojiao Yuan[1], Hynd Remita[1*]

[1] Institut de Chimie Physique, UMR 8000 CNRS, Université Paris-Saclay, 91405 Orsay, France

Abstract: Conjugated polymers (CPs) have been recently widely investigated for their properties and their applications in different fields including photocatalysis. Among the family of CPs, polypyrrole (PPy) has been the most extensively studied owing to its good environmental stability, high electrical conductivity, superior redox properties and easy synthesis. Besides, nanostructured polypyrrole-based nanomaterials are type of active organic materials for photocatalysis, which is one of their emerging applications. Nanostructuration of polypyrrole can reduce the electron-hole recombination because of short charge transfer distances and reactant adsorption, and product desorption can be enhanced owing to the high surface area offered by nanostructures. This review summarizes synthesis of different nanostructures based on π-conjugated polymer polypyrrole, and the latest developments for photocatalytic applications, including degradation of organic pollutants and hydrogen generation.

1. Introduction

Solar to chemical energy conversion provides a promising way to solve environmental and energy problems. Although solar light has the advantages of being cheap, abundant and clean, it is difficult to use solar energy effectively due to its intermittent nature. Half of the energy that sunlight reaches the surface of the earth comes from visible light photons (400 ~ 750 nm). However, most of inorganic

semiconductors (such as TiO_2 or ZnO) are only active under UV light, which constitutes 4~5% of the solar spectrum. Therefore, effective use of visible light is one of the biggest challenges in the field of photocatalysis. π-conjugated polymers (such as poly(diphenylbutadiyne) (PDPB), poly(3,4-ethylenedioxythiophene) (PEDOT), polypyrrole (PPy), poly(3-hexylthiophene) (P3HT)) can be considered as organic semiconductors, and have many inherent advantages, making them competitive alternatives to inorganic semiconductors for photocatalytic applications.[1, 2] First of all, organic semiconductors generally show very high absorption coefficients. In addition, narrow band gap and unique π-conjugated system of organic semiconductors make them easy for photogenerated charge carriers' separation, and the strong polarity can achieve effective charge transfers of both positive and negative charges, which is essential to initiate photoredox reactions.

An emerging and promising research topic consists in the development of organic semiconductors for photocatalytic applications and in particular for transformation of small molecules. Benefiting from the immense potentialities of solution processable organic semiconductors in the field of organic photovoltaics,[3] a lot of attention is put to exploit the photophysical and electrochemical properties of these materials in the solar to fuel driven chemistry. In 1980, Shirakawa et al. introduced for the first time polyacetylene at a photoelectrode for solar energy conversion.[4] The conjugated polymer poly(ρ-phenylene) was first reported for photocatalytic application in 1985 (see the timeline in **Fig.1**)[5]. In the presence of trimethylamine (TEA) or diethylamine, the radiation of an aqueous suspension of poly(ρ-phenylene) ($\lambda > 290$ nm) leads to the photocatalytic H_2 generation. In 2009, Domen and Antonetti discovered that graphitic carbon nitride g-C_3N_4 (melon) acts as a photocatalyst for the hydrogen evolution reaction in the presence of a sacrificial electron donor, and without any co-catalyst.[6] This

first reports inspired the research on polymeric photocatalysts in the past decade, including covalent organic frameworks (COF),[7-9] covalent triazine-based frameworks (CTFs) pyrene-based conjugated microporous polymers (CMPs) and conjugated poly(azomethine) networks.[10-15]

It has been demonstrated that conjugated polymer nanostructures such as poly(diphenylbutadyine)(PDPB),[16] poly(3,4-ethylenedioxythiophene)(PEDOT),[17] poly(3-hexylthiophene) (P3HT)[18] and polypyrrole (PPy)[19] (synthesized by controlled polymerization in soft templates made by hexagonal mesophases) are very active photocatalysts for water treatment under UV and visible light, with an activity under visible light overcoming that of a plasmonic Ag/TiO_2 taking as a reference.[19] These organic semiconductors show very high absorption coefficients and narrow band gaps (with absorption in the visible or near IR range), high stability and high carrier mobility. Their unique π-conjugated systems help photogenerated charge carriers' separation, and the strong polarity can achieve effective charge transfers, which are essential for initiating photoredox reactions.

Despite the great progress made in the pursuit of highly efficient organic photocatalysts, there are still considerable efforts necessary to understand their photocatalytic properties, and important progresses to achieve to increase the photocatalytic yields. In addition, although typical conductive polymers have been widely investigated, there are a few systematic reports on the performance, synthesis and application of conjugated polymers.

PPy has been studied in great details because of its good electrical conductivity, redox properties and environmental stability. The monomer (pyrrole, Py) is easily oxidized, water soluble and commercially available. It has been synthesized for the first time in 1912,[4] and its conductive property

was discovered in 1977.[4] PPy nanostructures (NSs) have a wide range of applications such as in batteries,[20] sensors,[21] photovoltaics,[22] self-cleaning surfaces,[23] etc.[24] However, it is only in 2019 that the first studies reported photocatalytic applications of bare PPy NSs.[19, 25, 26] In this review, we will introduce various synthesis strategies of PPy nanostructures (chemical polymerization, electrochemical polymerization and radiolytic polymerization) and PPy-based nanocomposites for photocatalytic applications (**Fig. 2**). More importantly, we will also focus on introducing the polymerization mechanisms, physical and chemical properties of PPy, and synthesis of different PPy nanostructures. Finally, the review concludes with the challenges and suggestions for improving the performance of nanostructured polypyrrole-based photocatalysts.

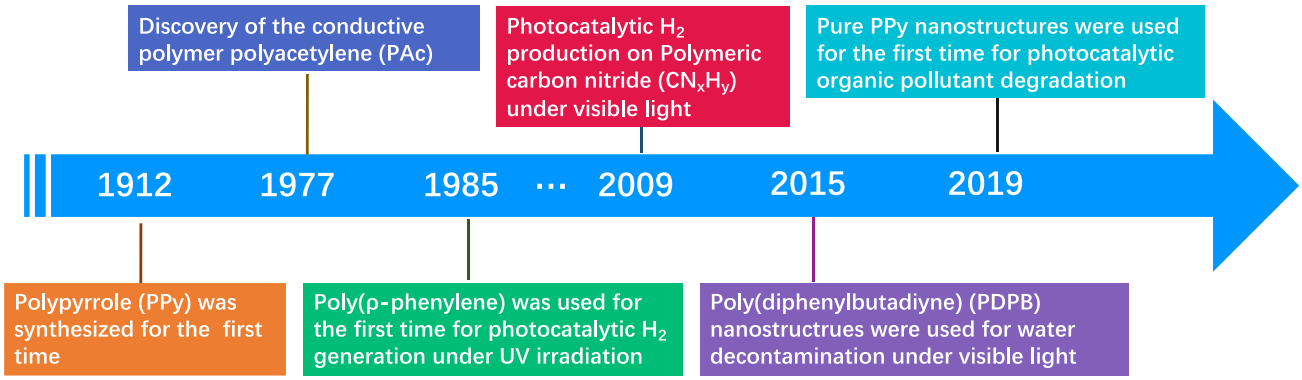

Fig.1. Timeline showing the key developments in photocatalytic applications using conjugated polymers.[5, 6, 16, 19, 25, 27]

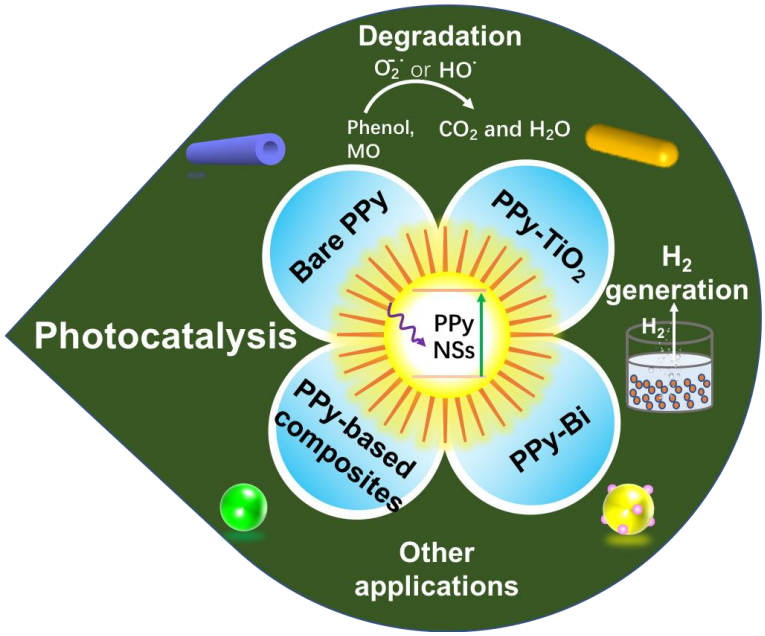

Fig. 2. Overview of polypyrrole nanostructures (PPy NSs) for various photocatalytic applications.

2. Chemical structures and the nature of electronical conductivity of PPy

π-conjugated polymers are considered as organic semiconductors and consist of a linear series of overlapping p_z orbitals with sp^2 or sp hybridization, thereby forming a conjugated chain of delocalized electrons.[28] Polypyrrole is one of the easiest conducting polymers to synthesize and one of the most stable. One-dimensional or two-dimensional PPy structures can be obtained depending on the synthesis conditions. The one-dimensional structure mainly refers to polymerization at the α–α positions (low oxidant concentration). On the other hand, the two-dimensional structure is mainly polymerized at α–β position (high oxidant concentration) (**Fig. 3**).[29]

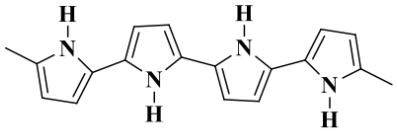

α-α polypyrrole

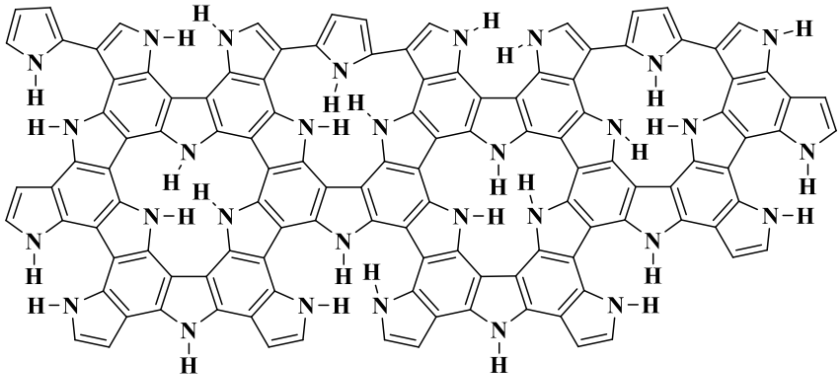

α-β polypyrrole

Fig. 3. One-dimensional (α- α) and two-dimensional (α-β) polypyrrole structures.[29]

Neutral (undoped) bulk polypyrrole is a dielectric material with a bandgap of 4 eV. After oxidation (doping), the π-electrons are removed from the HOMO (the highest occupied molecular orbital) to LUMO (the lowest unoccupied molecular orbital). The bandgap is reduced to less than 2.5 eV, and the polymer becomes a semiconductor.[30] PPy conduction is of particular interest for the mechanism of charge transfer.[31] The charge carriers are formed by polarons and bipolarons doping. Chemically speaking, the formation of polarons is equivalent to the formation of radical cations and of bipolarons, to dications (**Fig.4**). The polarons and bipolarons in PPy are extended structures, distributed in three to four monomer units of the chain. Polymers doping is accomplished in a variety of ways: chemical, electrochemical or photochemical doping, as well as by charge injection at the metal–insulator–semiconductor (MIS) interface.[32] The conductivity of PPy depends on the number of carriers and

charge carriers' mobility, which varies greatly depending on its synthesis conditions. Higher mobilities will occur with higher crystallinity, better orientation, and defect-free materials.[33] The main changes in conductivity usually occurs in the early stages of doping.[31, 34]

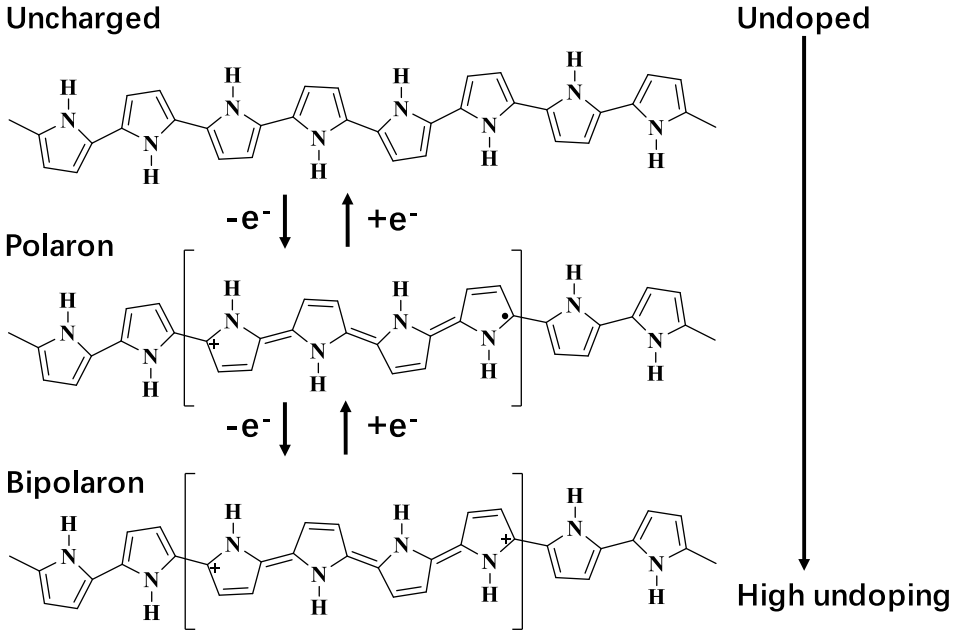

Fig. 4. Proposed structures for polarons and bipolarons.[35]

3. Synthesis of polypyrrole (PPy) nanostructures

PPy was for the first time synthesized in 1912.[25] Polymerization of pyrrole monomers (Py) into PPy can be achieved by traditional chemical oxidation (using for example $K_2S_2O_8$, $FeCl_3$, H_2O_2)[36] or electrochemical methods.[37] Chemical polymerization usually provides powdery PPy, and can be easily scaled up. Other polymerization methodologies have been also developed such as photo-induced synthesis[38] or radiolysis.[39] Although the polymerization technologies of chemical and electrochemical

methods are quite different, the first step of polymerization corresponds to the preliminary oxidation of Py monomers into their ionic form.

In addition, nanostructured conjugated polymers are attractive as advanced nanomaterials due to their performance and versatile applications. By using chemical and electrochemical polymerization, 0D-1D or 3D- nanostructures (NSs) of PPy such as nanoballs, nanorods, nanotubes, nanobowls or nanoclips can be obtained using hard or soft templates or structure-guiding agents (such as methyl orange).[40]

3.1 Chemical polymerization

Polymerization of Py occurs steadily in the presence of an oxidant (such as $FeCl_3$, ammonium persulfate (APS) or H_2O_2).[33, 41] Halogens and organic electron acceptors were also used as oxidants to synthesize PPy.[42, 43] Besides, there are many factors such as the nature of the solvent and the oxidant, initial Py/oxidant ratio, reaction duration and temperature, which can affect the yield and the conductivity of PPy.[44] For example, the optimized Fe(III)/Py ratio is 2.4 for a yield in PPy of about 100%. Changing the initial ratio of the reactants affects the yield, but not the chemical component nor conductivity.[45] The shorter times of polymerization and lower temperatures, (0 ºC ~ 5 ºC), the better conductivity of PPy is obtained.[46] When the oxidant is $FeCl_3$, the overall reaction is as follows (equation 1):[31]

$$n\ C_4H_5N + (2+y)n\ FeCl_3 \rightarrow (C_4H_5N)_n^{y+}\ ny\ Cl^- + (2+y)n\ FeCl_2 + 2n\ H^+ + 2n\ Cl^- \quad \text{(equation 1)}$$

where y is the doping level of PPy, and usually the value of y is between 0.20 and 0.33 for PPy. If oxygen is not counted, the reaction of Py with $FeCl_3$ can be presented as follows (equation 2):[44]

$$n\ C_4H_5N + 2.33\ n\ FeCl_3 \rightarrow (C_4H_5N)_n^+ + 0.33\ n\ Cl^- + 2.33\ n\ FelCl_2 + 2\ n\ H^+ + 2\ n\ Cl^- \quad \text{(equation 2)}$$

One chlorine atom can accept one electron (e^-) from three Py unites to be a doped anion.

PPy nanostructures of different shapes can be obtained using templates or surfactants as explained in the next paragraphs.

3. 1.1 PPy nanospheres

The main disadvantages of templated and seeded growth synthetic routes are that the use of templates or seeds can add cost and complexity to the synthesis, and removing the template or the seeds can affect the physical properties of the nanostructures. Emulsion and dispersion polymerizations often need external emulsifiers or stabilizers, which can be difficult to remove. Hong et al. reported a facile way to synthesize uniform nanometer-sized PPy based on water-soluble polymers and metal cations in aqueous solutions without any surfactant nor template (**Fig. 5a-c**) [47]. The metal cation (Fe^{3+}) was used as an oxidizing agent to initiate the chemical oxidation polymerization of Py, and the facile process provides a great possibility for mass production of PPy NPs. Liao et al. synthesized water-dispersible PPy nanospheres with size less than 100 nm without any template, surfactant, nor functional dopant via introducing 2,4-diaminodiphenylamine as initiator into a reaction mixture containing Py monomer, an oxidant (such as $FeCl_3$), and hydrochloric acid (HCl) (**Fig. 5d**). [48] The size and morphologies of PPy NPs are dependent on the initiator and oxidant concentrations.

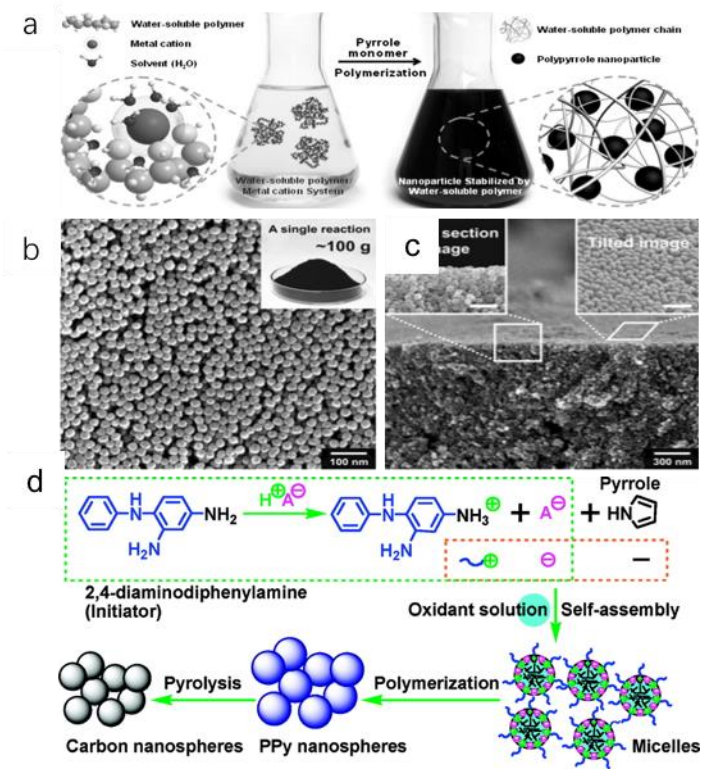

Fig. 5 (a) Schematic diagram of synthesis process of water-soluble PPy. **(b)** SEM image of PPy nanoparticles. **(c)** Tilted and cross-section SEM images of the PPy nanoparticles stacked on a substrate (scale bar: 100 nm).[47] Copyright 2010 Wiley-VCH. (**d**) Formation mechanism proposed for PPy and carbon nanospheres.[48] Copyright 2010, American Chemical Society.

3.1.2 PPy hollow spheres

PPy hollow spheres providing some immediate advantages over their solid counterparts were used for various applications because of their relatively low densities. During the past decades, different synthetic methods were developed for the PPy hollow spheres preparation, however, the most efficient procedure is based on template-assisted synthesis, e.g., polystyrene latex spheres (PS) [49, 50], SiO_2 spheres [51], metal and metal derivatives as templates (such as Au, Fe, AgCl) [52-54], PPy hollow spheres could be subsequently achieved via removal of the templates. For example, D. Su et al. used poly(methyl methacrylate) (PMMA) nanoparticles (NPs) as templates to synthesize PPy hollow

spheres [55]. **Fig. 6a** is a schematic diagram, which illustrates the synthesis of PPy hollow nanospheres. The PMMA can be washed away with acetone. SEM and TEM images showed the as-prepared PPy retained the spherical shape of the templates with a homogeneous size distribution, without shrinkage nor structural deformation (**Fig. 6b-c**). X. Liu et al. demonstrated a simple in situ synthetic method to obtain SiO_2/PPy core–shell particles (**Fig. 6d**). PPy hollow spheres were obtained after removing the SiO_2 template [56] (**Fig. 6e**); Their size and thickness were dependent on the size of SiO_2 and the added volume of Py monomer.

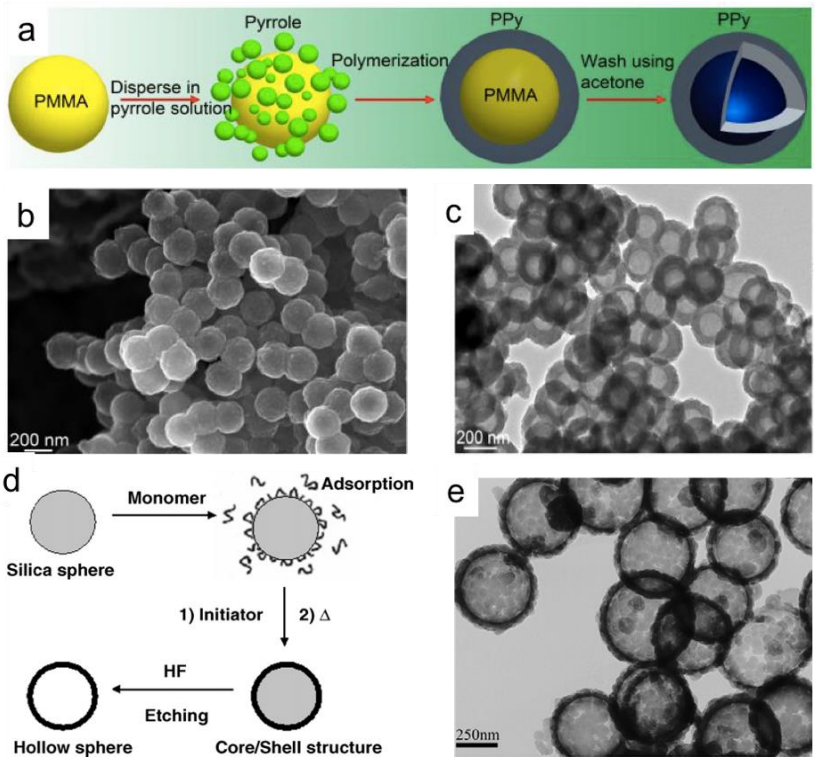

Fig. 6. (a) Schematic diagram of the synthesis of PPy hollow nanospheres. **(b)** FESEM images of as-prepared PPy hollow nanospheres. **(c)** TEM image of as-prepared PPy hollow nanospheres;[55] Reproduced from Ref. 49 with permission from the Royal Society of Chemistry. **(d)** The formation mechanism of SiO_2/polypyrrole core–shell structure particles and PPy hollow spheres; **(e)** TEM image of PPy hollow spheres.[56] Copyright 2007 Elsevier B.V.

3.1.3 PPy nanowires and nanotubes

One dimensional nanowires and nanotubes have attracted much attention in recent years due to the high sensitivity to surface effects and a configured channel for carrying charge and exciton efficiently.[57] The unique geometrical advantages and properties promote the various applications of nanowires and nanotubes. Generally, synthesis of PPy nanotubes or nanowires is based on templates such as anodic aluminum oxide (AAO),[58] structure-guiding agent MO,[59] V_2O_5 nanofibers.[60]

For example, Zhang et al. synthesized one-dimensional PPy nanotubes using $FeCl_3$ as oxidant and V_2O_5 nanofibers as sacrificial hard templates (**Fig. 7a-b and e-f**) and the synthetic doped PPy nanotubes with hollow holes can spontaneously reduce the noble metal ions to nanoparticles (Ag, Au, Pd etc.) on the tubes' surface (**Fig. 7c-d**).[60, 61] Methyl orange (MO) was for the first time reported by Yang et al. in 2005 as a simple and easily accessible structure-guiding agent to synthesize PPy nanotubes.[62] MO with a planar hydrophobic section and hydrophilic edge group ($-SO_3^-$) is soluble in water, and possesses anionic and no surfactant characteristics in aqueous solution due to the absence of critical micelle concentration. At room temperature (25°C), MO can dimerize and form oligomers at a concentration of 1 mM and 5~10 mM, respectively.[62] Complexation can be obtained when an organic compound (such as phenol or a dye) and a flocculant (Fe^{3+} or Al^{3+}) are together. In the work reported by Yang et al., $FeCl_3$ was used to suppress the electrostatic repulsions between MO aggregates and/or reacts with negatively charged aggregates of MO in solutions, which induces destabilization of the charged particles and formation of amorphous aggregates.[62] PPy hollow nanotubes were obtained in high yield using $FeCl_3$-MO reactive self-degraded template, which the outer and inner diameters are

about 70 nm and 50 nm, respectively. Notably, when the oxidant $FeCl_3$ is replaced by ammonium peroxysulfate (APS), no tubular precipitates are observed after mixture with MO. Yan et al. reported synthesis of PPy nanotubes (PPy-NTs) with uniform diameters (~100 nm) by in situ chemical polymerization of Py with $FeCl_3$ and MO as oxidant and dopant, respectively. They showed that the diameter of the PPy-NTs can be controlled by adjusting the concentration of the reactants, the types of solvents and the reaction temperature (**Fig. 7g-h).** Granular PPy NPs were obtained in the absence of MO.[63]

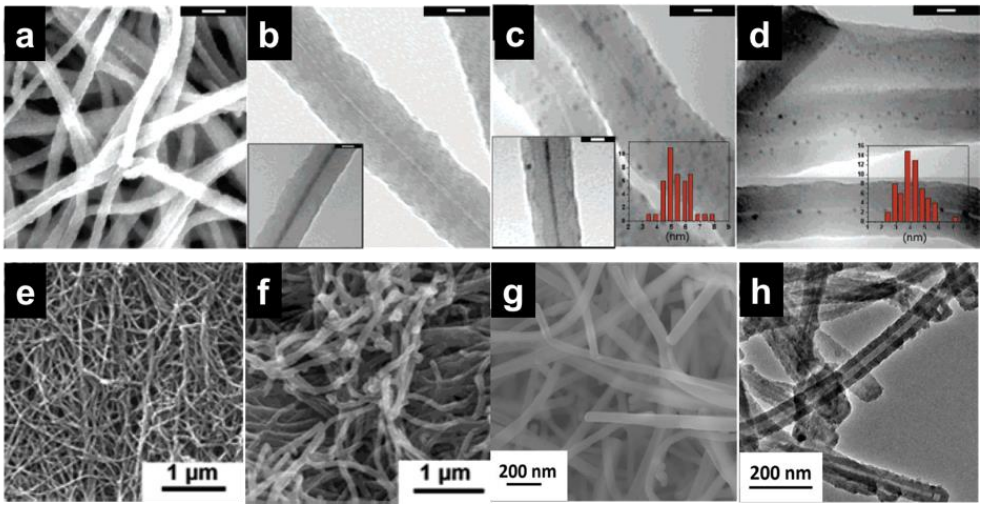

Fig. 7. Polypyrrole·Cl nanotubes: (**a**) SEM, as synthesized. (**b**) TEM, as synthesized showing a hollow tube. Inset: TEM showing a pore filled with V_2O_5. (**c**) TEM, Ag nanocomposite. Insets: coaxial cable of Ag and particle size distribution (**d**) TEM, Au nanocomposite;[60] Copyright 2005 American Chemical Society. SEM images of polypyrrole·Cl nanofibers synthesized in ethanol/$FeCl_3$ using V_2O_5 as the seed. Prior to the reaction, V_2O_5 was stirred in ethanol for (**e**) 30 min and (**f**) 12 h;[61] Copyright 2004 American Chemical Society. (**g**) SEM images of PPy-NTs obtained in the presence of MO, (**h**) TEM images of PPy-NTs obtained in the presence of MO.[63] Copyright 2017 ESG (Belgrade, Serbia).

3.1.4 Other nanostructures of PPy

Other two-dimensional PPy nanostructures have been developed in the recent years. PPy nanorings obtained by using a soft template ($(CTA)_2PdBr_4$ complex), while the Pd complex was synthesized via the reduction reaction between $PdBr_4^{2-}$ and the monomer (Py) and finally Pd nanoparticles supported on PPy (**Fig. 8a**).[64] Liu et al. described for the first time synthesis of 2-D nanoclip structures of PPy by using an oxidative template composed of cetrimonium cations and peroxydisulfate anions in the presence of CTAB (**Fig. 8b**). The diameter of the homogeneous nanoclips was in the 50~70 nm range.[65] Monodispersed nanobowl sheets of PPy were synthesized by using polystyrene spheres at the aqueous/air interface as templates via chemical polymerization (**Fig. 8c**). These PPy nanobowls can be easily lifted-off and deposited, in full size, on any flat substrate.[66] L.M. Santino reported on a modified vapor-phase synthesis of polypyrrole nanofibers (PPy), which can conformably coat 3D fibrillar substrates such as hard carbon papers. This facile polymerization method provides the opportunity to deposit PPy NSs onto many electrochemically active materials, but it may not be stable at high temperatures (**Fig. 8d-e**).[67]

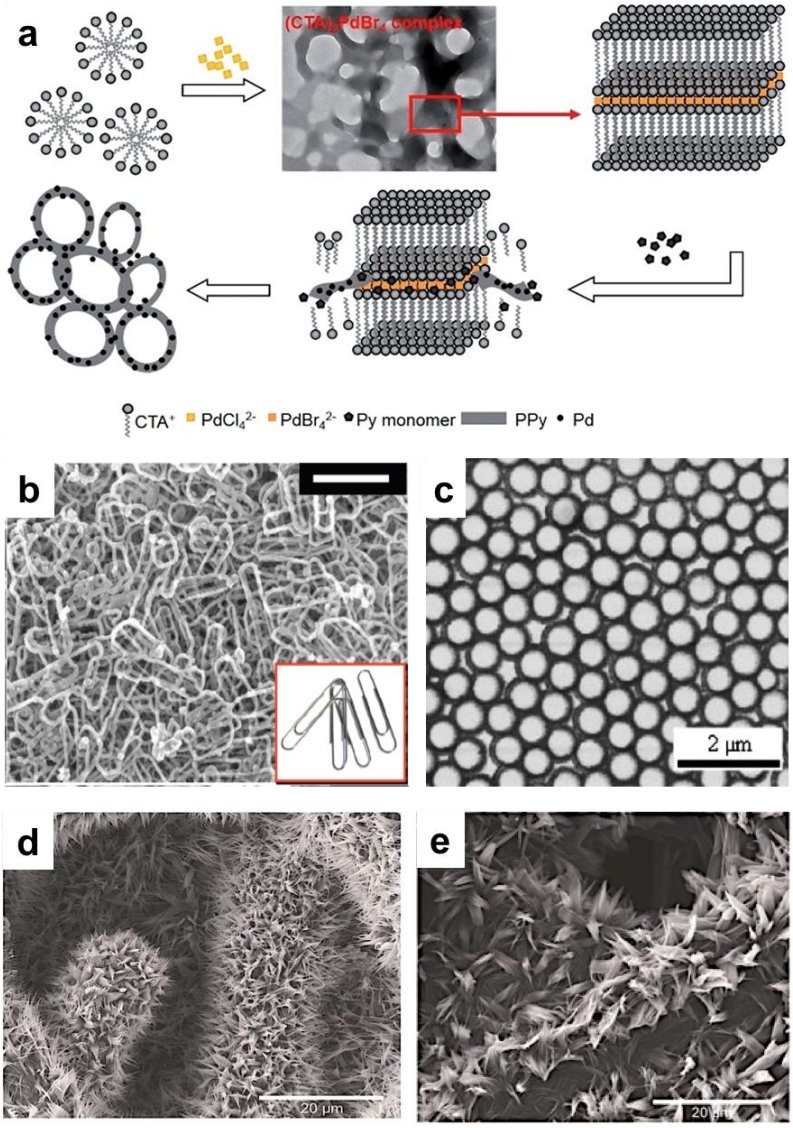

Fig. 8. (**a**) Schematic diagram of the fabrication of PPy-Pd composite nanorings.[64] Reproduced from Ref. 58 with permission from the Royal Society of Chemistry. (**b**) SEM images of PPy·Cl nanoclips (scale bar, 1 μm; inset, digital picture of paper clips).[65] Copyright 2010 American Chemical Society. (**c**) SEM images of the PPy-CSA nanobowl sheet.[66] Copyright © 2006 WILEY-VCH. (**d**) SEM of unwashed PPy after vapor phase polymerization onto a hard carbon paper substrate, (**e**) Upon washing in 6 M HCl and methanol, the fibers relax yet remain separated.[67] Reproduced from Ref. 61 with permission from the Royal Society of Chemistry.

3. 2 Electrochemical polymerizations

Electropolymerization limits the reactions on the surface of the electrodes, and the PPy (prepared by this method) normally grows on the surface of the electrode as a film. Typically, PPy NSs grow along with the orientation of the electric field to form special structures.[68]

The mechanism of electropolymerized PPy is still controversial although different mechanisms have been proposed so far by Diaz,[69] Kim,[70] Pletcher[71] and Reynold.[72] Among them, Diaz's mechanism is the most frequently encountered in the literature. The reaction process of this mechanism is as follows:[69, 73] In the first step, the oxidation of Py leads to a radical cation formation (Scheme 1) and several resonance forms of this cation are expressed in Scheme 2:

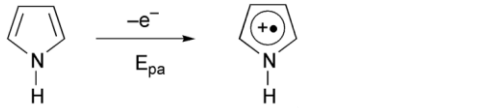

Scheme 1

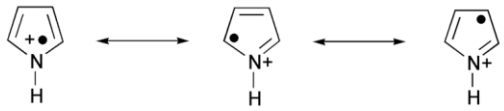

Scheme 2

Two unpaired electron density in the α-position of dimerizes by resonance to form a dihydromer dication (Scheme 3), and the two protons loss leads to formation of a dimer (Scheme 4).

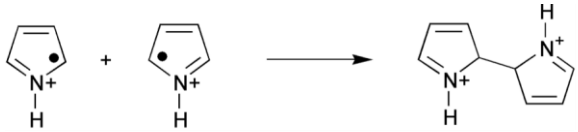

Scheme 3

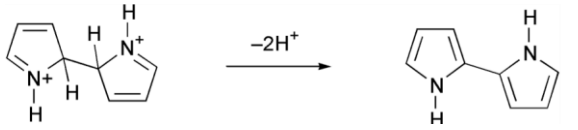

Scheme 4

The bipyrrole is more easily oxidized due to the its lower oxidation potential than the one of the monomer (Scheme 5).

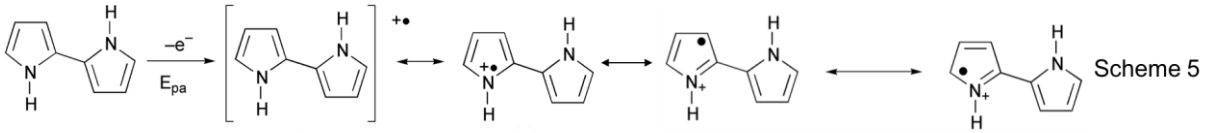

Scheme 5

The resonance cation form reacts with a monomer to form the trimer dication, and then deprotonates to obtain the neutral trimer (Scheme 6). Trimer α- and β-positions can be coupled with the following oligomers even if β-position could not be accessible sterically and α-coupling will predominate (Scheme 7), the longer the length of the chain, the higher number of β-bands formed.

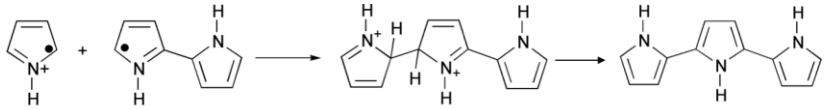

Scheme 6

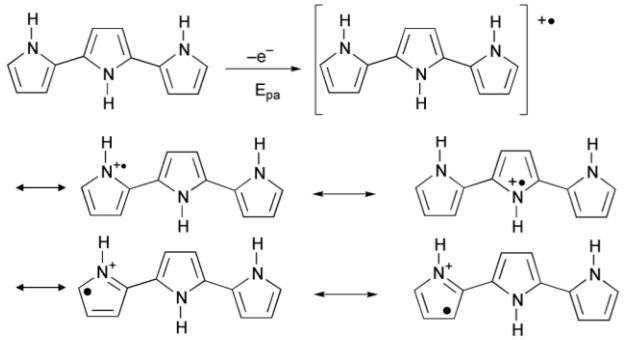

Scheme 7

The propagation continues in the same order: oxidation, coupling and deprotonation until the final polymer product is obtained (Scheme 8).

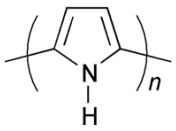

Scheme 8

Indeed, Diaz et al. were the first to synthesize PPy by electropolymerization. The method features a combination of several successive reactions such as radical cation formation, radical coupling and deprotonation. However, some steps like propagation and termination are hard to investigate. Besides, many electropolymerization parameters also influence the property of polymerization. [69, 71]

3. 2.1 PPy nanowires and nanotubes

The electrochemical polymerization of Py favors formation of PPy bulk materials such as conductive films. D.-H. Nam successfully fabricated PPy nanowires with a one-step process by cathodic electropolymerization without templates nor chemical additives. The electrochemically generated NO^+ was utilized to oxidize neutral Py monomers, making it possible to use oxidable metal substrates such as Cu and Ni. The synthesized nanowires are directly deposited on the Cu substrate as a thin film, and the kinetics of Py polymerization in cathodic electropolymerization is highly influenced by the radical cations' reactivity. The results showed that PPy nanospheres initially deposited on the Cu substrate gradually changed to nanowire structures in the form of a thin film. The growth kinetics of PPy nanowires was studied by analyzing the effect of the electrolyte and synthetic time (**Fig. 9a-c**), which shows that the polymerization process of pyrrole is very sensitive to the reactivity of radical cations.[74] J. Xing et al. showed a facile approach to construct antimicrobial peptide functionalized PPy nanowires array conductive electrodes for bacterial environment electrical signal detection application (**Fig. 9d-e**). They introduced an antimicrobial peptide (AMP) immobilized PPy nanowires array conductive electrode (PNW-AMP) using facile electrochemical deposition, and further molecular immobilizing process through the existing dopant (dopamine) as an anchor.[75] PPy nanotubes can be synthesized using sacrificial templates (α-Fe_2O_3 nanowires grown on the steel substrate), and then α-Fe_2O_3 nanowire template was removed by H_3PO_4 solution at constant current of 5 mA cm^{-2} (**Fig. 9f**).[76]

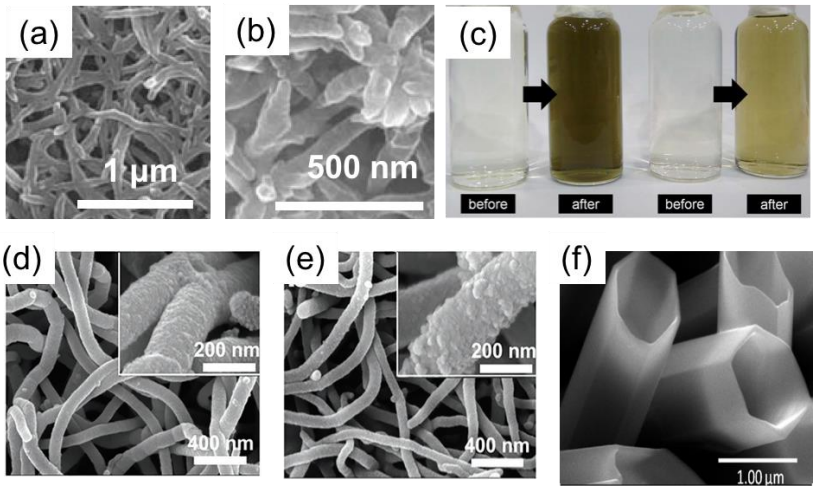

Fig. 9 (a) SEM images of the polypyrrole nanowires synthesized by cathodic electropolymerization at -0.6 V_{SCE} for 10 min from an aqueous solution containing 0.2 M $NaNO_3$ and 0.8 M HNO_3 with concentrations of pyrrole 0.20 M, **(b)** at 0.25 M pyrrole and 0.8 M HNO_3 with 0.2 M $NaNO_3$, **(c)** the changes in electrolyte color before and after cathodic electropolymerization at -0.6 V_{SCE} for 10 min: (left) 0.025 M pyrrole, 0.2 M $NaNO_3$ and 0.8 M HNO_3 and (right) 0.2 M pyrrole, 0.2 M $NaNO_3$ and 0.8 M HNO_3;[74] Reproduced from Ref. 68 with permission from the Royal Society of Chemistry. **(d)** SEM image of constructed PPy nanowire electrode (PNW) surface. **(e)** SEM image of AMP immobilized PPy nanowire electrode (PNW-AMP) surface. Insets in (d) and (e) were high magnification images.[75] Copyright 2019 Wiley-VCH. **(f)** high-magnification SEM image of polypyrrole nanotubes.[76] Copyright 2011, American Chemical Society.

3. 2. 2 PPy microsuckers and microcontainers

Patterned conducting polymers have attained promising applications in various fields. A general strategy for the fabrication of patterned PPy, with precisely controlled microstructures (e.g., polypyrrole microsuckers) was developed by regulating the solid/liquid/gas triphase interface and the electrochemical polymerization. The PPy microsuckers were successfully deposited on micropillars with different top shapes (circular pillars, spindle pillars and hexagonal pillars) (**Fig. 10 a**).[77]

L. Qu et al. prepared PPy microcontainers with morphology like cups, bottles and bowls by electrochemical oxidation of Py in the aqueous solution of β-NSA (β-naphthalene sulfonic acid, an anionic surfactant),[78] camphorsulfonic acid,[79] or polyelectrolyte[80] (**Fig. 10b-g**). These surfactants coated on the surface of gas bubbles and resulted in forming "soap bubbles", which are negatively charged. They can assemble on the surface of working electrodes under a positive potential during the electropolymerization. These microcontainers with diameters of 20~100 nm and thickness of 10~150 nm stand upright on the working electrode surface. Then, Y. Gao et al. developed a microdroplet template for the electrochemical synthesis of PPy microcontainers by combining the layer-by-layer (LBL) technique (**Fig. 10f**).[81, 82] In the synthesis process, Py was dispersed as microdroplets in aqueous $LiClO_4$ solution by sonication following assembled on the ITO electrode decorated with multilayers of poly(diallyldimethylammoiun chloride) and poly(styrene sulfonic acid) at a positive potential. Finally, the well-ordered PPy microcontainers formed by the polymerization of the outermost layers of the droplets with the diameter of 1~10 μm, which are smaller than those of the microcontainers prepared by the "soap bubble" template strategy.

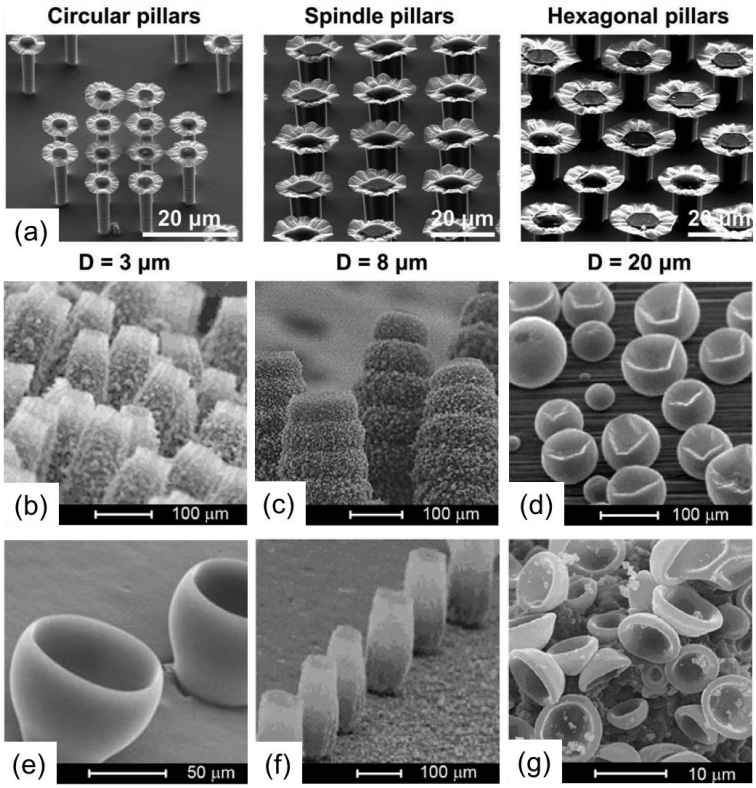

Fig. 10 (a) ESEM images of PPy microsuckers deposited on different micropillars, including circular pillars, spindle pillars and hexagonal pillars;[77] Copyright 2018 Wiley-VCH. SEM images of PPy microcontainers and microspheres synthesized by electrochemical polymerizations. (**b**) Microcontainers doped with camphorsulfonic acid;[78] (**c**) Microcontainers doped with poly (styrenesulfonic acid); Copyright 2003, American Chemical Society. (**d**) Microcontainers doped with camphorsulfonic acid and prepared by the CV technique;[79] Copyright 2004, Elsevier. (**e**) Arranged microcontainers on patterned electrodes; (**f**) Microspheres doped with naphthalene sulfonic acid;[80] Copyright 2004 Wiley. (**g**) Microcontainers prepared by electrochemical growth of PPy on layer by layer (LBL) film modified electrode.[82] Copyright 2006, Elsevier.

Electrochemical polymerization provides many advantages compared to chemical methods. Firstly, the obtained product is an electroactive film, which attaches to the electrode surface and shows high conductivity. Secondly, it is easy to control the mass and the thickness of the film; Thirdly, the film can be controlled directly in the synthesis process.[31] Using electrochemical polymerization, various complex structures can be achieved.

3. 3 Polymerization by radiolysis

Radiolysis is the interaction of high energy radiation (γ-rays, X-rays, electrons or ions beams) with matter. It is a powerful technique to synthesize metal nanoparticles, polymer nanostructures and composite nanomaterials.[83, 84] The interaction of high-energy radiation (γ-rays, X-rays, accelerated electrons or ions beams) with polar solvents such as water generates free radicals (solvated electrons e^-_s, $H^{\bullet}$, $HO^{\bullet}$) homogeneously in the solution, H_3O^+ and molecular recombination products (H_2 and H_2O_2).[85, 86]

The process of free radical formation in the case of radiolysis of water is as follows (**equation 3**):[87]

$$H_2O \xrightarrow{\gamma-radiation} e^-_s, H_3O^{\bullet+}, H^{\cdot}, HO^{\cdot}, H_2, H_2O_2 \text{ (equation 3)}$$

Solvated electrons and $H^{\bullet}$ radicals are strong reducing species while $HO^{\bullet}$ are strong oxidative radicals E^o ($HO^{\bullet}/H_2O$) = 2.2 V (vs SHE).[88] These radicals can be used for reduction or oxidation reactions.

S. Remita et al. have developed a methodology based on radiation chemistry to synthesize conducting polymers in aqueous solutions and halo-methane solvents (such as DCM, CH_2Cl_2) radiolysis.[89-94] The oxidative or reducing radicals used for polymerization are induced by solvent radiolysis, therefore no external oxidative (or reducing) chemicals are needed to initiate the polymerization as in the case of chemical method. The team synthesized PEDOT polymers for the first time using γ radiolysis in water.[90] In this way, the synthetic procedure is easy and environmentally friendly. In other words, water is used as solvent without addition of chemical

oxidants or reductive agents, the oxidative or deducing radicals are induced by water radiolysis. PPy spherical NSs were synthesized by γ-ray irradiation in water under N_2O atmosphere without any templates. While hydroxyl radical is a very oxidative species, N_2O was not only used to scavenge solvated electrons, but also to produce more oxidative $HO^{\bullet}$ radicals ($e^-_{aq} + N_2O + H_2O \rightarrow HO^{\bullet} + HO^- + N_2$). Py was polymerized into PPy due to the hydroxyl radicals produced by water radiolysis (**Fig. 12a-b**).[19, 39] On another hand, spherical PPy polymer nanostructures were recently radiosynthesized in dichloromethane, the polymerization being initiated by the generated chloromethyl ($CH_2Cl^{\cdot}$) and dichloromethyl ($CHCl_2^{\cdot}$) radicals under N_2 during DCM radiolysis, and a higher yield of monomer oxidation as well as a greater efficiency of polymerization can be obtained. Radiolysis provides a facile way to synthesize monodisperse PPy nanospheres.[93, 95]

Wang et al. reported synthesis of PPy nanospheres with uniform size about 30.5 nm through γ-ray irradiation in an acidic aqueous solution of Py, and the monodispersed PPy NPs showed high-efficient NIR photothermal conversion for cancer therapy (**Fig. 12c-d**).[96]

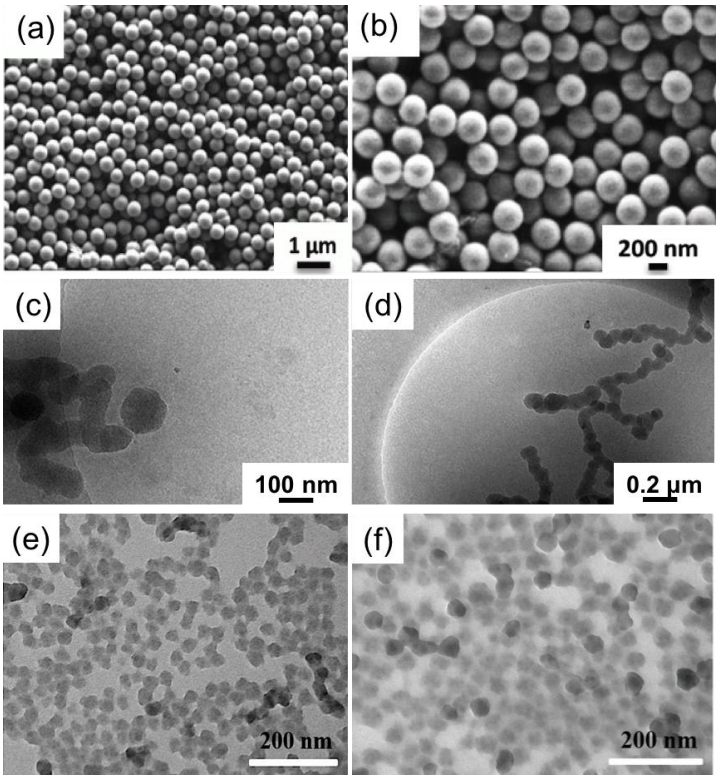

Fig. 12 (**a-b**) SEM images of PPy-NSs-γ.[19] Copyright 2019, Elsevier. Cryo-TEM images of radio synthesized PPy (γ-PPy) at 72 kGy. (**c**) Nanostructures of γ-PPy; (**d**) full view of chaplets of γ-PPy.[39] Copyright 2014, American Chemical Society. TEM images of the products prepared from γ-ray radiation on an acidic aqueous solution of Py at different pH: **e**) pH = 1; **f**) pH = 0.8.[96] Copyright 2017 Wiley-VCH.

3. 4 Photopolymerization

There are few reports about photopolymerization of Py. In photopolymerization process, photogenerated electron transfer plays an important role. Generally, metal complexes (such as ruthenium, cobalt and copper complexes) have been used as photosensitizers and electron acceptors.[97] C.R. Martins et al. prepared PPy/Ag composite via photopolymerization process. The strategy was to use the transition metals ions assisted by UV light to polymerize monomers, and in the same time Ag ions are reduced and incorporated to the PPy matrix (**Fig. 13a**).[98] Ag/PPy core/shell NPs with a

diameter of 60 nm were obtained by one-step UV-induced polymerization in the presence of PVP (polyvinylpyrrolidone), which acts as stabilizer ((**Fig. 13b**).[99] PPy films can be deposited on silicon substrates by spin coating. These films were polymerized by UV light (172 nm wavelength), and the structures are affected by UV irradiation and exposure time. The UV-photo processing includes two stages: photopolymerization and then PPy film surface etching and modification.[38]

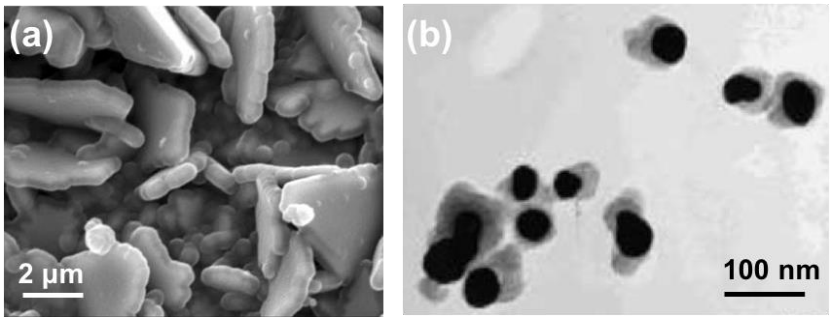

Fig. 13 (a) SEM of polypyrrole film on glass substrate for exposure of the monomer solution 72 h,[98] **(b)** TEM images of silver/polypyrrole core/shell particles centrifuged.[99] Copyright 2005, Elsevier.

4. Polypyrrole nanostructures for environment and energy applications

Conjugated polymers with their unique electron system (one-dimensional delocalized conjugated structures), excellent optical, electrical and electrochemical properties are used in various applications (such as actuators, supercapacitor electrodes, ablation of cancer cells, fuel cells and catalysis). Especially, conjugated polymers have attracted much attention for photovoltaic cells and photocatalysis due to their high conductivity, stability, charge carriers' mobility, broad absorption in the visible light and excellent electrochemical performance. For example, thin films of conjugated polymer are one of the potential alternatives of crystalline silicon photovoltaic cells, which can provide

electricity at a lower cost than crystalline silicon solar cells and could be achieved on a large scale.[100] In addition, conjugated polymer nanostructures also emerge as new photocatalysts very efficient under visible light.[16-19, 101] X. Yuan et al. reported for the first-time the high photocatalytic activity of bare PPy NSs for water treatment under visible light and that the PPy NSs are stable with cycling (**Fig. 14a-c**). The NSs were synthesized by chemical oxidation in soft templates (PPy-NSs-c), gamma irradiation (PPy-NSs-γ) and without any template by chemical oxidation (PPy-bulk). The authors demonstrated that nanostructuration is a key factor for the high photocatalytic activity of PPy-NSs.[19] Nanostructuration provides large surface area, which is beneficial for photocatalysis and less defects compared to the bulk counterpart, these defects acting as recombination sites decreasing the photocatalytic activity. Interesting, the HOMO, LUMO energy levels and the band gap can be tuned by the control of the polymerization degree of the conjugated polymer and its nanostructuration.[19,16,17] The proposed photocatalytic mechanism was shown in **Fig. 14d**. Separated photogenerated charge carries participate in redox reactions during the photocatalytic process and superoxide and hydroxyl radicals are very active species to oxidize organic pollutants into CO_2 and H_2O (complete mineralization of the pollutant is achieved).

It is worth noting that the photocatalytic activity of PPy NSs was shown to depend on the polymer morphology, particles size, as well as on optical and chemical states.[19] It has been shown recently that PPy polymers radiosynthesized in dichloromethane (DCM) solvent (PPy_{DCM}) exhibit very high photocatalytic activity for water treatment compared to PPy synthesized by radiolysis in water (PPy_{H2O}), and this activity is comparable to that of the best conjugated polymer based photocatalysts synthesized within hexagonal mesophases. [88] This activity was explained by longer chain length, the

doping state of PPy synthesized in CH_2Cl_2, by its very small optical band gap (1.30 eV), and also by its large extended absorption band from the UV to the near infrared region. [88] These photocatalysts were found to be very stable with cycling.

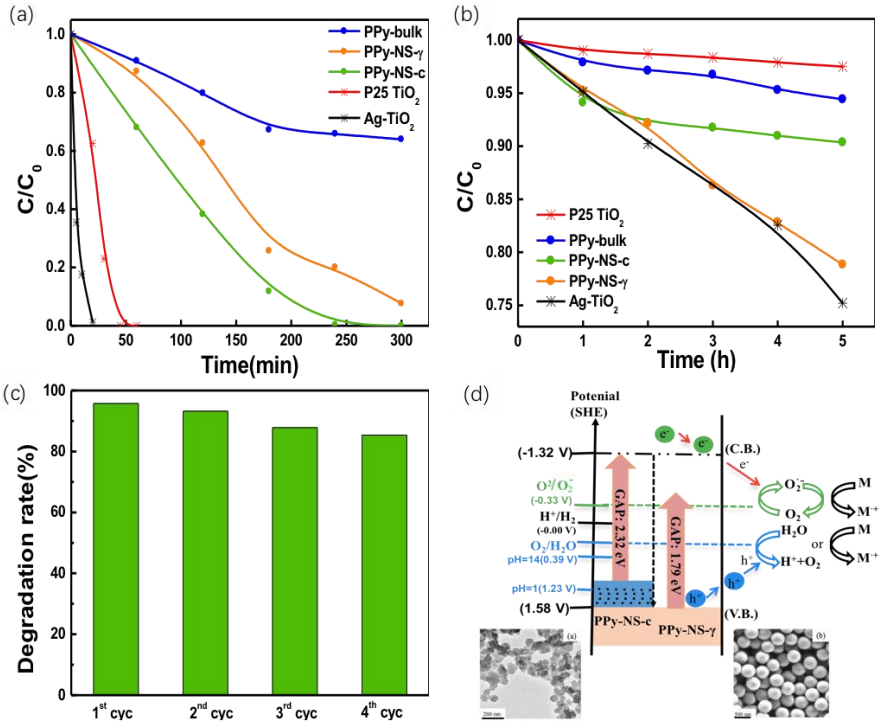

Fig. 14 Degradation rates of phenol in the presence of as-prepared samples of PPy under UV-Vis **(a)** and visible light irradiation **(b)**; **(c)** Photocatalytic activity of PPy-NS-c with cycling. **(d)** Possible photocatalytic mechanism with charge separation in PPy nanostructures with electron reducing oxygen and the hole oxidizing water.[19] Copyright 2019 Elsevier.

In addition, a great deal of efforts has been devoted to increase the photocatalytic efficiency and to extend the light absorption range of TiO_2. Among these approaches, formation of semiconductor heterojunction is an efficient way to enhance the photocatalytic properties. According to the electronic affinity and bandgap of semiconductors, heterostructures can be divided into three types: type I (straddling gap), type II (staggered gap), and type III (broken gap) (**Fig. 15**).[102] Formation of type II heterostructures is the most investigated and efficient way to decrease the recombination of charge

carriers for enhanced photocatalytic activity for degradation of organic pollutants and water splitting. On the other hand, the formed heterostructures can effectively increase the utilization efficiency of solar energy owing to the synergetic absorption of different semiconductors.

PPy-based heterojunctions can play a pivotal way for photocatalytic applications owing to the narrower band gap and broadened light absorption in the visible region.

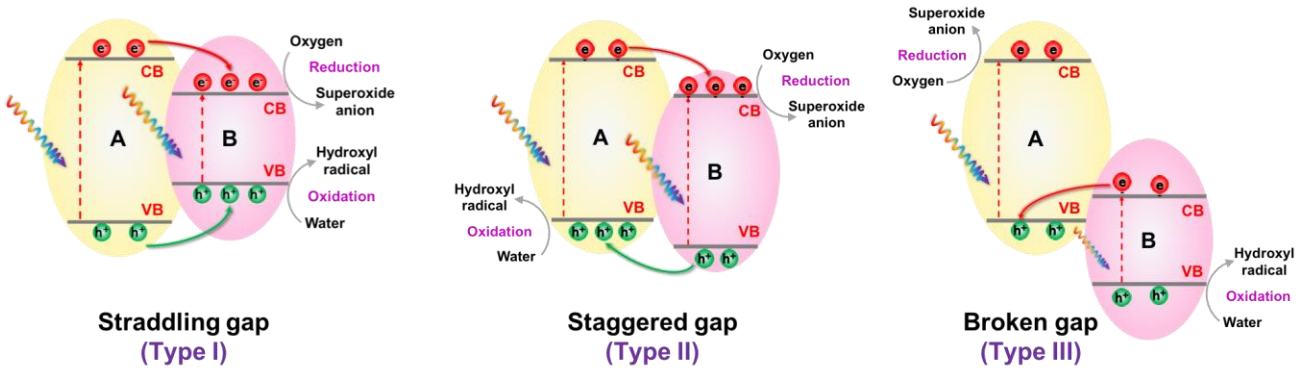

Fig. 15 Schematic energy band diagram of three types of semiconductor heterojunctions.[102]

4. 1 Polypyrrole-based composites for water treatment

PPy can be combined with inorganic semiconductor nanomaterials for application in photocatalysis. In organic-inorganic nanocomposites, organic materials are usually used to support and separate inorganic nanomaterials, and improve their properties (such as electronic and catalytic properties) by allowing a higher surface area to volume ratio.[103]

4. 1.1 Polypyrrole-based binary composites for water treatment

a. PPy/TiO_2 composites

Organic-inorganic semiconductor nanocomposites exhibit both the performance of pure organic and inorganic semiconductor materials, and synergistic effects can be obtained for some applications. It has been shown that PPy decorated with inorganic metal oxides presents large visible light absorption and good photocatalytic activity. For example, PPy/TiO_2 nanocomposite particles showed enhanced photocatalytic activity for degradation of pollutants in water (MO and phenol were used as model pollutant) under visible light irradiation[104, 105]; PPy-TiO_2 composite films at the air-water interface presented higher photocatalytic activity than a suspension of PPy-TiO_2 for MO and MB degradation.[106] Surface molecularly imprinted polymers do not only show strong affinity towards target contaminants, but also facilitate mass transfer owing to the accessible sites and the PPy/TiO_2 nanocomposites exhibit high efficiency for photodegradation of MO.[107] X. Yuan et al. modified commercial P25 TiO_2 with nanostructured PPy (PPy_{NS}) (prepared in soft templates formed by hexagonal mesophases[108]) by sonication (5 min) and followed by 2 h stirring in ethanol for water and air treatment.[109] Compared with PPy_{bulk}-TiO_2 (in this case PPy prepared without any template in water had larger size that PPy_{NS}), the nanocomposite shows a significant improvement in photocatalytic performance under visible light for photodegradation of organic pollutants in water and in air (MO and phenol were taken as model water pollutants and toluene as air pollutant) (**Fig. 16a-c**). This enhancement of photocatalytic activity was attributed to the nanostructured PPy and to the formation of heterojunction at the interface between PPy_{NS} and TiO_2, which promotes the charge carriers'

separation (**Fig. 16d**). Another study showed that PPy/TiO_2 can also be used for photocatalytic degradation of polyethylene plastic under sunlight irradiation.[110]

In the PPy/TiO_2 system, PPy (narrow band gap) can harvest visible light matching the energy levels of the inorganic semiconductor, and subsequently inject photogenerated electrons into the CB of TiO_2, which facilitates the electron transfer and decreases the recombination of charge carriers. Time resolved microwave conductivity (TRMC) technique was used to study the dynamics of charge carriers in the TiO_2-based composite. Under visible excitation (450 nm), the TRMC signal of PPy_{NS}-TiO_2 was higher than that of bare TiO_2, which indicated the longer life time of charge carriers due to less recombinations in the PPy_{NS}-TiO_2 composite (**Fig. 16c**). The photocatalytic activity can be improved by the formation of a heterojunction between PPy and TiO_2 and this activity is stable with cycling.

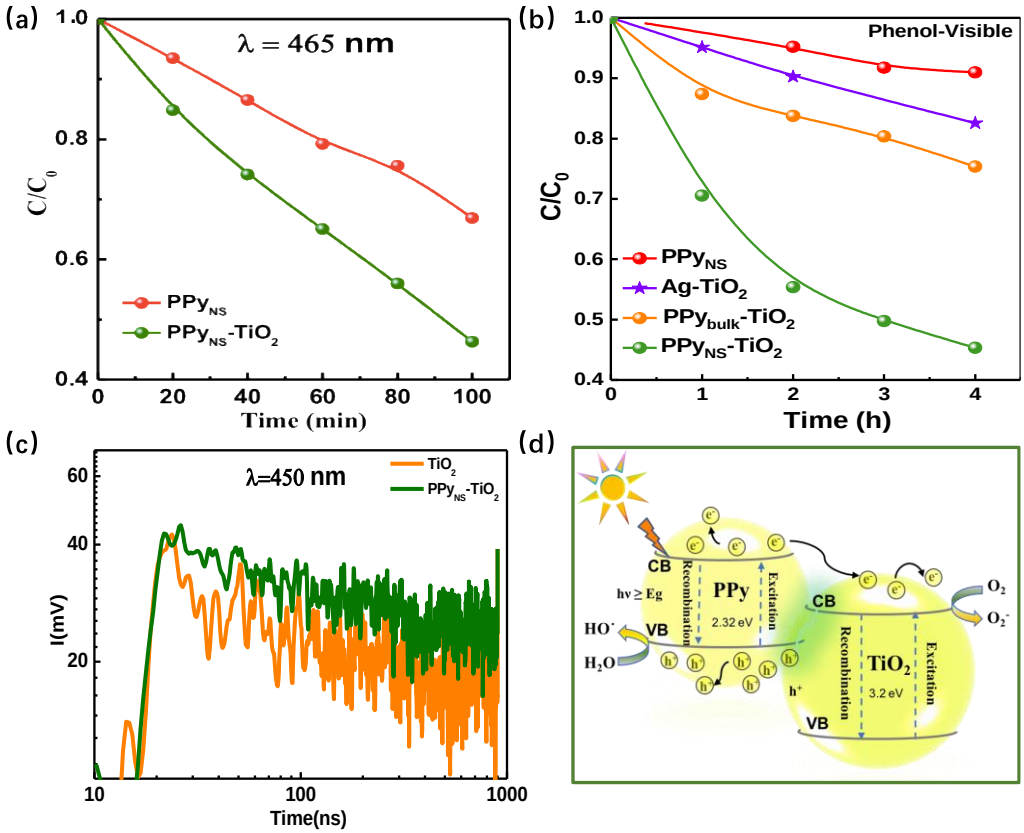

Fig. 16 (**a**) Photocatalytic activity of PPy_{NS} and PPy_{NS}-TiO_2 for the toluene degradation under λ = 465 nm irradiation. (**b**) Photocatalytic degradation rate of phenol under visible light. (**c**) TRMC (time resolved microwave conductivity) signals of PPy_{NS}-TiO_2 and TiO_2 at excitation wavelength 450 nm irradiation. (**d**) Proposed photocatalytic mechanism for the PPy_{NS}-TiO_2 system and charge transfer mechanism under visible light.[109] Copyright 2020, Elsevier.

b. PPy modified with bismuth-based photocatalyst

Bismuth-based semiconductors such as Bi_2O_3,[111] Bi_2WO_6,[112] $BiVO_4$,[113] $Bi_2O_2CO_3$[114] present efficient photocatalytic performances in water depollution.

Bismuth oxyhalides BiOX (X = Cl, Br, I) with unique layered structure featuring $(Bi_2O_2)^{2-}$ layers and inter-grown X^- layers, which exhibit good photocatalytic performance for pollutant degradation,

are believed as the promising photocatalysts. Composite materials based on BiOX with a heterojunction with another semiconductor such as TiO_2 show improved photocatalytic activity than the bare materials.[115] In case of BiOX-PPy, computational calculations showed that oxygen vacancies (formed due to strong interactions between BiOCl and polypyrrole (PPy)) work as sites to activate O_2 molecules, and therefore the relative barrier energies of NO oxidation were significantly reduced due to the O_2 activation process. BiOCl/PPy was more efficient for photocatalytic NO removal than that BiOCl, and the activity increases with the amount of PPy, and BiOCl/PPy photocatalysts exhibited enhanced activity for NO oxidation (NO_3^-) and inhibited toxic NO_2 generation (**Fig. 17a-b**).[116] Likewise, X. Liu et al. fabricated a hybrid BiOBr-Ag-PPy (BAP) system, which showed superior photocatalytic activity in degradation of triphenylmethane dye (malachite green) and organic pollutant (phenol). In BAP system, PPy and BiOBr serve as electron and hole donors, and Ag NPs act as electron mediators, building a bridge for charge transfer and separation, which significantly enhances the photocatalytic performance (**Fig. 17c**).[117] PPy with BiOI nanosheet (PPy-BiOI) by a facile in situ precipitation strategy at room temperature presented high photocatalytic activity for industrial depollution (bisphenol A and 2,4-dichlorophenol) and antibiotics (tetracycline hydrochloride and chlortetracycline hydrochloride).[118] The composite formation induces broadening of light absorption to visible light, and the loading of PPy with bismuth-based photocatalysts plays an important role in the photoactivity and 5%PPy-BiOI shows the best activity compared with 0.5%, 2% and 7% PPy. Enhanced visible light photocatalytic activity of Bi_2WO_6 photocatalyst modified with different amounts of polypyrrole (PPy) was synthesized by in situ deposition oxidative polymerization of pyrrole. The photocatalytic activity of PPy/Bi_2WO_6 composite modified with different amounts of PPy are in the following orders: 0.5

wt% > 0.75 wt% > 0.25 wt% > 1 wt%, excess of PPy on the surface of Bi_2WO_6 induces a decrease in the photocatalytic performance, which is attributed to the increased absorbance and scattering of photons and shield the light to reach the surface of Bi_2WO_6 photocatalyst. However, appropriate amounts of PPy existing on Bi_2WO_6 exhibited great influences on improving the photocatalytic activity of Bi_2WO_6.[119] In addition, PPy/$Bi_2O_2CO_3$ composite synthesized by hydrothermal method presents enhanced activity for rhodamine B (RhB) degradation under UV light irradiation.[120]

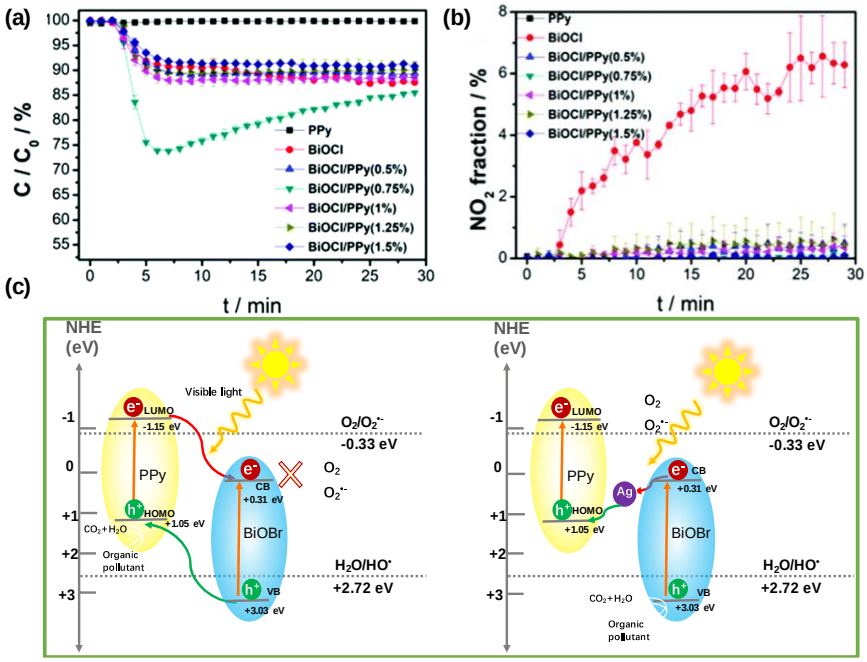

Fig. 17. NO removal (**a**) and NO_2 production (**b**) of BiOCl and BiOCl/PPy composites under visible light,[116] Reproduced from Ref. 109 with permission from the Royal Society of Chemistry. (**c**) Schematic of charge carriers transfer in BiOBr-PPy and BiOBr-Ag-PPy.[117]

c. Other composite materials based on PPy for photocatalysis

ZnO microrod arrays and polypyrrole (PPy) flexible composite films show a remarkably increased photocatalytic activity under visible light. In this integrated heterogeneous structure, the upper PPy coating shell serves as a photosensitizer for the ZnO-based photocatalysis, while the lower PPy base layer facilitates electron transport to the substrate and mechanically reinforces the ZnO microrod arrays. Under visible light, this facile structure achieves much higher photocatalytic efficiency in comparison with bare ZnO microrod arrays or PPy films for methylene blue (MB) degradation at a rate of 0.22%/min.[121]

Fe_2O_3 has a smaller band gap compared to TiO_2 and ZnO, and F. A. Harraz reported mesoporous heterostructure α-Fe_2O_3/PPy for MB degradation at room temperature under UV irradiation. After 20 min, the MB was completely degraded in the presence of optimized 10% Py (volume ratio).[122] Very recently, heterojunction nanocomposite PPy@Fe_2O_3 showed high photocatalytic activity in photoreforming of micro plastic to hydrogen and other value-added organic products.[123] A visible-light-driven three-dimensional PPy/$Zn_3In_2S_6$ nanoflower photocatalyst was developed, which presents very high activity for photoreduction of Cr(VI), (100% Cr(VI) (50 mg/L) reduction in 24 min) and MO (10 mg/L) degradation (99.4% degradation in 25 min).[124] Another photocatalyst, Ag_2MoO_4/PPy nanocomposite, was in situ synthesized and utilized it as a photocatalyst for the degradation of MB (99.9%) and ciprofloxacin (CIP) drug (99.8%), and reduction of Cr (VI) (99%) within 10 min. The composite obtained a higher photocatalytic performance than PPy and Ag_2MoO_4 alone.[125] Non-metal oxides nanoparticles were also combined to PPy. Carbon dots (CDs) (prepared using waste

watermelon seeds (**Fig. 18a-b**)) were deposited on polypyrrole grafted chitosan, and the composite material exhibits enhanced photocatalytic activity for degradation of toxic 2-chloro phenol (2-CP).[126]

Polyoxometallates (POMs) (metal (Mo^{VI}, Ta^{V}, Mo^{V}, W^{VI}, V^{V}, Mo^{V}) (which are oxide polyanion clusters linked together by shared oxygen atoms to form well-defined frameworks) can store and exchange a large amount of electrons, and have been widely investigated in photocatalysis.[127] However, investigations of PPy/POM-based photocatalysts for water depollution are rare. X. Xu et al. reported loading of PPy on a transition metal coordination polymer (TMCP)/POM via a facile in situ polymerization process, and the PPy/$CuSiW_{12}$ composite shows enhanced photocatalytic activity for degradation of RhB under visible light (**Fig. 18c-f**).[128]

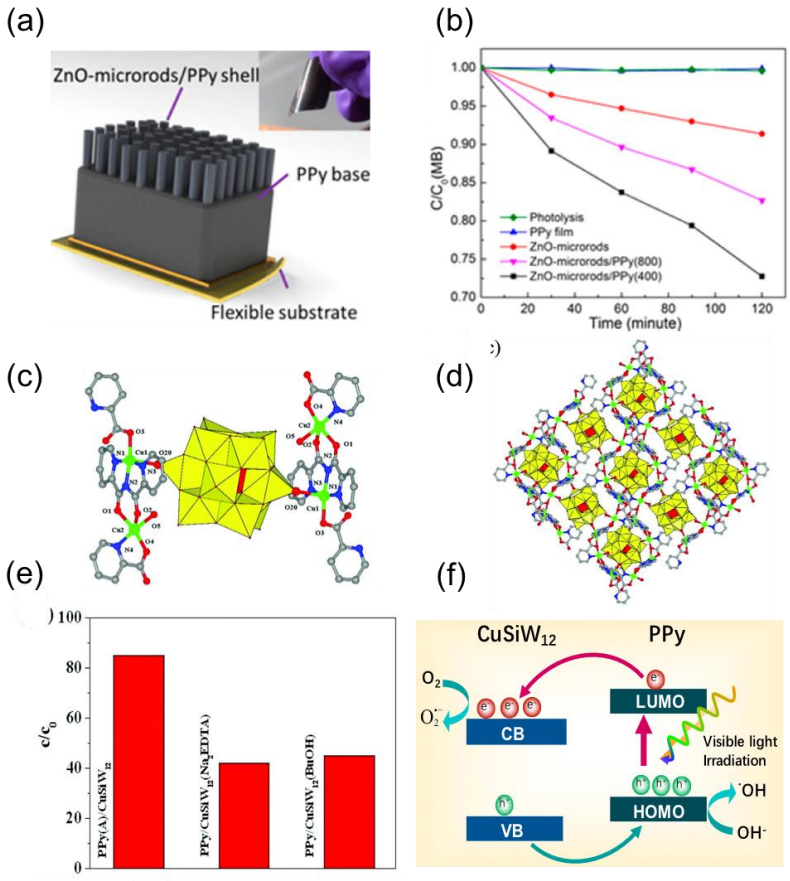

Fig. 18 (a) PPy/PEG-borate was electrodeposited onto the ZnO microrod arrays; **(b)** Degradation rates of methylene blue by photolysis under visible light.[126] Copyright 2019 American Chemical Society. **(c)** Fundamental unit of $CuSiW_{12}$; **(d)** 2D framework of $CuSiW_{12}$; **(e)** Photocatalytic efficiency of PPy/$CuSiW_{12}$ and **(f)** Diagram of the photocatalytic mechanism for PPy/$CuSiW_{12}$ under visible light.[128] Reproduced from Ref. 120 with permission from the Royal Society of Chemistry.

4. 1. 2 Polypyrrole-based ternary composites for water treatment

PPy-Ag-TiO_2 ternary composite formed by a shell of PPy, a core of TiO_2 decorated with Ag NPs showed an important increase of the photocatalytic activity compared with that of single- and two-component systems. The enhanced photocatalytic activity may be due to the synergistic effect of PPy, Ag and TiO_2 nanostructures in the ternary system (**Fig. 19a-b**).[129] BiOBr-Ag-PPy photocatalyst shows excellent activity and stability for decomposition of malachite green.[117] Another example of composite photocatalyst is TiO_2–polydopamine (PDA)/PPy/cotton, which presents an excellent activity with a ~96% degradation of methyl orange (MO) under simulated solar irradiation over 3 h, and the degradation efficiency still maintained up to 60% after 10 cycling tests, which showed that the TiO_2-PDA/PPy/cotton exhibited a good photocatalytic stability.[130] It has been shown that the PDA/PPy structure can enhance the photocatalytic performance of TiO_2 by promoting the separation of photogenerated electron–hole pairs and decreasing charge recombination (**Fig. 19c-e**). Conductive polypyrrole–polyaniline/TiO_2 nanocomposites (PPy–PANI/TiO_2) prepared by in situ oxidative copolymerization of pyrrole and aniline monomers in the presence of TiO_2 exhibit high visible-light photocatalytic activity for degradation of 4-nitrophenol. [131] The efficiency of PPy–PANI/TiO_2 is owing

to its conductivity, conjugated structure, as well as to the synergy between polypyrrole, polyaniline and TiO_2. Ag_3PO_4-$BiPO_4$-PPy heterostructures (by co-precipitation hydrothermal technique and oxidative polymerization method) showed significantly improved photocatalytic activity for malachite green degradation.[132] Recently, Y. Lin et al. demonstrated that a spatial separation system of photogenerated carriers in Ag_3PO_4@MWCNTs@PPy composite presented excellent photocatalytic activity for the degradation of phenol (100% in 20 min) and tetracycline hydrochloride (100% in 5 min). Importantly, the small-sized Ag_3PO_4 showed higher photocatalytic activity than large-sized.[133]

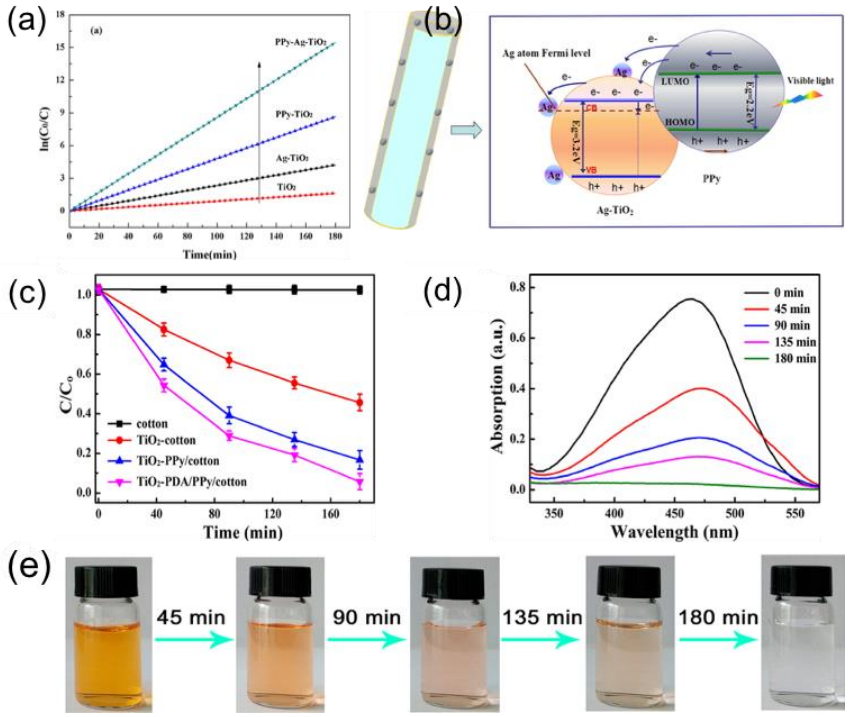

Fig. 19 (**a**) The visible-induced photocatalytic activity of different samples; (**b**) Postulated mechanism of the visible light-induced photo-degradation of acetone with PPy-Ag-TiO_2 nanocomposites.[129] Copyright 2013, American Chemical Society. (**c**) Photodegradation of MO with different samples under simulated solar power for 180 min; (**d**) UV−vis adsorption spectra showing photo degradation of MO with TiO_2−PDA/PPy/cotton under 1 kW m^{-2} illumination; (**e**) Pictures showing the color change of the MO solution containing TiO_2−PDA/PPy/cotton.[130] Copyright 2018, American Chemical Society.

4. 2 PPy-based composites for photocatalytic H_2 generation

Bare PPy NPs show very low activity for photocatalytic H_2 production because of the fast charge carriers' recombination and low catalysis kinetics. The introduction of a co-catalyst (such as Pt, Ni, NiO, PtNi,) NPs for photocatalytic hydrogen generation can reduce the activation energy of the reaction, provide active sites for proton reduction, and decrease the recombination of charge carriers, resulting in an improvement of the photocatalytic activity for hydrogen production. In addition, the amount and loading method of co-catalyst are also crucial factors for hydrogen generation. The co-catalyst metal NPs with uniform dispersion can enhance the hydrogen production. However, the investigation of PPy-based composites for photocatalytic hydrogen generation is still scarce.

X. Yuan et al. reported modification of PPy nanostructures with mono- and bimetallic (Pt, Ni, Pt-Ni) NPs induced by radiolysis. The modified PPy is very active for H_2 generation. Due to the effective separation of electron-hole pairs by nano-scale Pt, Ni and Pt-Ni particles and the enlarged absorption region of PPy NSs, the designed composite NSs exhibit excellent photocatalytic activity for H_2 production. Interestingly, the authors found that a 50/50 mixture of Ni and Pt shows an enhanced photocatalytic activity (664 μmol/h/g) compared with a pure Pt loading (341 μmol/h/g) or a pure Ni loading (52 μmol/h/g). The enhancement of hydrogen generation compared with that of the monometallic samples is owing to a synergetic effect between Ni and Pt: The presence of Pt induces better electron scavenging and higher $H^{\cdot}$ production, while the association with Ni promotes $H^{\cdot}$ recombination leading to higher H_2 production. (**Fig. 20a-b**).[101] Hydrogen production with Pt and PtNi modified PPy was very stable with cycling. Besides, Au NPs based multimetallic alloy deposited on

PPy nanofibers ($Au_{50}Pt_{24}Pd_{26}$/PPy) were also investigated (**Figure 1.19a**). The enhanced photocatalytic performance for $Au_{50}Pt_{24}Pd_{26}$/PPy is attributed to the localized surface plasmon resonance (SPR) of Au NPs, which probably leads to hot e^- migration from Au to the PPy. The effect of SPR can facilitate the charge carriers' formation and improve the e^-/h^+ separation (**Figure 1.19b**).[134] Copper NPs (Cu in its zero oxidation state or as oxides) are other promising cocatalysts and Cu is 6000 times cheaper than Au, has similar crystal structure and electronic configuration like noble metals.[135] Cu/PPy and Cu_2O/PPy heterostructures shows enhanced photocatalytic H_2 generation under visible light compared to pristine PPy.[136] PPy and Cu_2O can be excited under visible light irradiation, and charge carriers are generated. The photogenerated e^- migrate from the LUMO of PPy to the CB of Cu_2O, while the hole (h^+) transfer from the VB of Cu_2O to the HOMO of PPy (**Fig. 1.19d**). The formed heterostructure can markedly promote the charge separation and transfer, which induces enhancement of the photocatalytic activity.

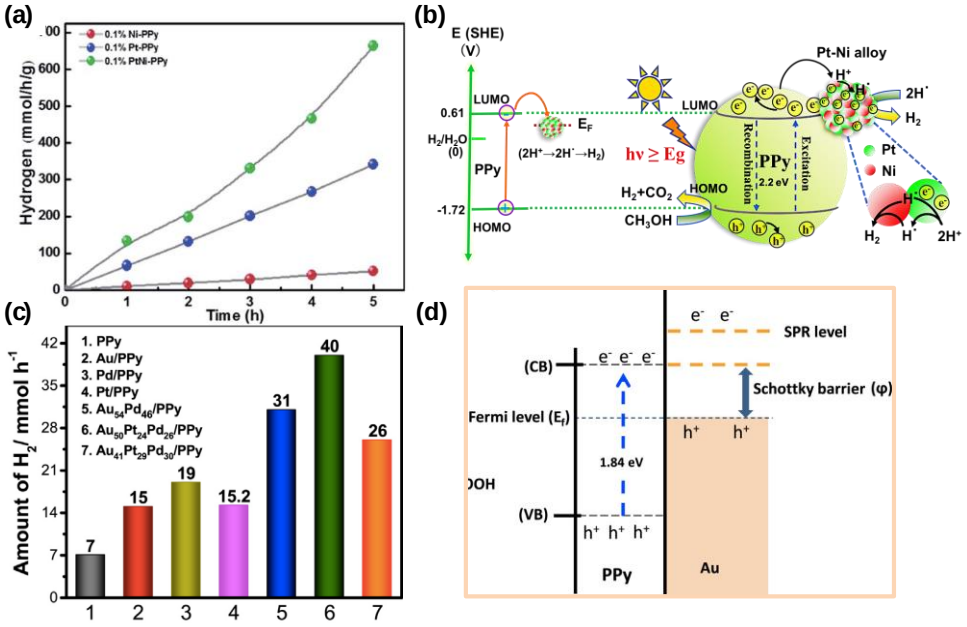

Fig. 20 (a) Photocatalytic H_2 generation rate with the same loading rate for different samples. **(b)** Proposed photocatalytic mechanism for hydrogen generation.[101] Reproduced from Ref. 94 with permission from the Royal Society of Chemistry. **(c)** The comparative data of H_2 generation rate after 60 min visible light illumination for bare PPy and PPy based nanohybrids. **(d)** Possible mechanism involved in the photocatalytic activity of Au/PPy NHs.[134] Copyright 2019, Elsevier.

Noble metals with lower Fermi level are efficient in electron trapping. Among these noble metals, Pt is the best candidate cocatalyst for hydrogen production due to its largest work function. T.A. Kandiel et al. reported an enhanced photocatalytic H_2 production on TiO_2 modified with Pt-PPy nanocomposites. Pt-PPy modified TiO_2 showed higher catalytic performance than that of Pt-TiO_2 under UV-vis illumination. A synergistic effect between Pt NPs and PPy results in a better charge carriers' separation (**Fig. 21a-b**).[137] N.M. Dimitrijevic synthesized TiO_2/polypyrrole nanocomposites by a simple one-step hydrothermal method. The composites are active under visible light irradiation driven by their morphology that is high concentration of 4.5 nm TiO_2 electronically coupled to 200-300 nm PPy granules. PPy acts as a visible-light photosensitizer, and the photoactivity of nanocomposite increases due to electron transfer from excited polypyrrole to TiO_2 nanoparticles, and further across the nanocomposite interface. TiO_2/PPy composite modified with Pt NPs showed high photocatalytic efficiency for H_2 generation (1 mmol H_2 $g_{catalyst}^{-1}$ h^{-1} wt% (Pt)). [138] PPy modified Pd-TiO_2 (TiO_2-Pd-PPy) showed higher H_2 generation rate (601 μmol/h) than TiO_2-Pd and TiO_2.[139] To avoid the use of noble metal NPs, some other cocatalysts were investigated for photocatalytic hydrogen production. CdS is one of the most efficient visible-light-driven photocatalysts due to its narrow band gap (2.4 eV), and its conduction band edge (more negative than the H_2O/H_2 electrode potential).[140] However modification with CdS should be considered with caution because of the toxicity of CdS and

Cd^{2+}, which can leach after contact of the nanomaterials with water. PPy/CdS photocatalyst obtained by in situ chemical polymerization with different dopants (sodium dodecylbenzene sulfonate (DBSNa), hexadecyl trimethyl ammonium bromide (CTAB) and sodium p-toluenesulfonate (TSNa)) were also investigated and PPy/CdS doped by TSNa presented the best photocatalytic activity for H_2 generation without noble metals under visible light irradiation compared to PPy doped by DBSNa and CTAB, and the rate of H_2 evolution was 4.4 times higher than that of CdS.[141]

In another hand, graphitic carbon nitride (g-C_3N_4), a metal-free semiconductor photocatalyst, when modified with cocatalysts, is also an efficient visible light-driven water-splitting catalyst for hydrogen evolution.[142] Y. Sui et al. prepared highly dispersed conductive polymer PPy (1.5 wt%) on C_3N_4, which exhibited enhanced photocatalytic activity for H_2 evolution compared with bare C_3N_4 from pure water under solar light.[143] Recently, different ternary hybrid nanostructures based on PPy-TiO_2 composites with controlled site modification with small Pt nanoparticles (2 nm Pt NPs induced by radiolysis) were fabricated (labeled as Pt-(PPy-TiO_2), (Pt-PPy)-TiO_2 and (Pt-TiO_2)-PPy, respectively). Pt-(PPy-TiO_2) presented the highest activity due to the effective electron transfer from PPy to Pt NPs and through TiO_2 to Pt, which resulted in more efficient separation of charge carriers and higher electron accumulation of Pt-(PPy-TiO_2) compared with (Pt-PPy)-TiO_2 and (Pt-TiO_2)-PPy (**Fig. 21c-d**). Furthermore, Pt NPs act as a cocatalysts for H^+ reduction and as a site for $H^{\cdot}$ recombination. The synergistic effect of the two electron transfer routes and formation of PPy-TiO_2 heterojunction facilitate the photocatalytic reaction process. The photocatalytic activity was found to be stable with cycling. This work opens new perspectives for the rational design of ternary composite

materials to promote charge transfers, thereby efficiently converting solar energy into chemical energy.[144]

Although conjugated polymer-based catalysts have achieved considerable development for photocatalytic hydrogen generation, the investigation of PPy-based composite photocatalysts is still scarce, for example, appropriate structures and sizes of PPy-based photocatalysts, suitable co-catalysts and optimized loading rate, reproducibility, decreasing or eliminating the use of rare and expensive elements etc.

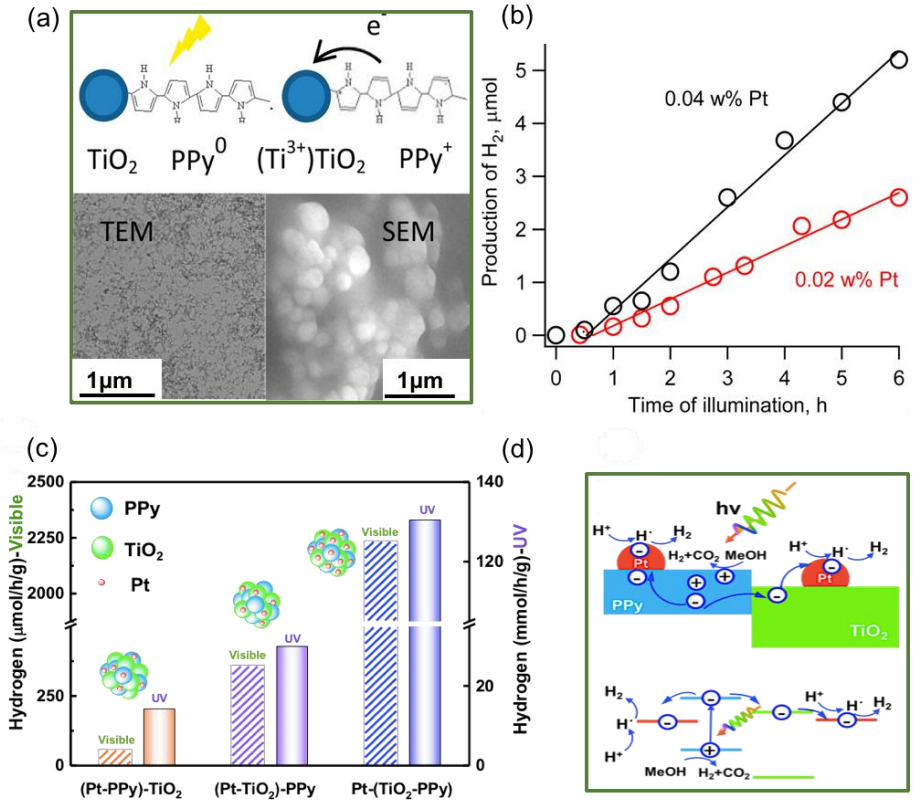

Fig. 21 (**a**) Electron transfer route of PPy-TiO_2, TEM and SEM images of PPy-TiO_2; (**b**) Yield of H_2 production over time. Two solutions with different weight percent of Pt were tested. Both contained a total of 24 mg of TiO_2/PPy–Pt nanocomposites and 6.4 mmol of TEA.[137] Reproduced from Ref. 129 with permission from the Royal Society of Chemistry. (**c**) H_2 evolution by using 0.5 g l^{-1} modified catalyst, 1.0 wt% Pt and polypyrrole, respectively, 75 ml aqueous

methanol solution; (**d**) Scheme for photocatalytic activity of TiO_2 modified with Pt–polypyrrole nanocomposites.[144] Copyright 2021, Elsevier.

5. Conclusions and perspectives

In this review, we have summarized various preparation methods (chemical, electrochemical, radiolytic and photo- polymerization) of conjugated polymer polypyrrole to obtain different nanostructures (such as nanoballs, nanotubes, nanoclips, etc.) with or without templates, and the application of polypyrrole-based nanomaterials in photocatalysis (especially for photocatalytic degradation of organic pollutants and H_2 generation). Although PPy has been studied for a long time, there are still different questions to be addressed. Firstly, more research is needed to understand the chemical structures during the polymerization since PPy is easy to be overoxidized, and the relationship between changes of chemical structure (such as polymerization degree, doping) and the photocatalytic performance should be further studied. Secondly, it is important to develop simple and effective methods to synthesize large-scale, long-term stable, and more efficient PPy-based materials for practical applications. Properties of these materials can be optimized through rational syntheses. Furthermore, modification of PPy nanostructures with cocatalysts (such as Fe, Ni, Cu or NiO, CuO, Sn) and another semiconductor (TiO_2, $BiVO_4$ or C_3N_4) to form heterojunctions will change the molecular structure, band gap, charge carriers' mobility and active sites, which plays an important role in various photocatalytic applications such as water splitting, water oxidation and CO_2 reduction. Their possible band gap engineering to optimize light absorption and the charge transfer pathways should be further studied. Finally, PPy nanostructures and PPy-based composite materials are very promising for application in photocatalysis. These materials can be very active for solar light harvesting, and can

have applications in air and water treatment, water splitting, hydrogen and solar fuels' generation,[145] water oxidation,[146, 147] and self-cleaning surfaces,[148, 149] and studies are conducted to understand the photocatalytic mechanisms involved in PPy-nanostructures and PPy-based nanocomposites. These materials are also promising for CO_2 reduction[145, 150] and valorization, methane conversion,[151] and NO_x reduction.[152]

Conflict of Interest Statement: On behalf of all authors, the corresponding author states that there is no conflict of interest.

Reference:

1. S. Ghosh, H. Remita and R. N. Basu, *Visible Light-Active Photocatalysis: Nanostructured Catalyst Design, Mechanisms, and Applications*, 2018, 227-252.
2. S. Ghosh, *Visible-light-active photocatalysis: nanostructured catalyst design, mechanisms, and applications*, John Wiley & Sons, 2018.
3. B. Kippelen and J.-L. Brédas, *Energy & Environmental Science*, 2009, **2**, 251-261.
4. H. Shirakawa, S. Ikeda, M. Aizawa, J. Yoshitake and S. Suzuki, *Synthetic Metals*, 1981, **4**, 43-49.
5. S. Yanagida, A. Kabumoto, K. Mizumoto, C. Pac and K. Yoshino, *Journal of the Chemical Society, Chemical Communications*, 1985, 474-475.
6. X. Wang, K. Maeda, A. Thomas, K. Takanabe, G. Xin, J. M. Carlsson, K. Domen and M. Antonietti, *Nature materials*, 2009, **8**, 76-80.
7. L. Stegbauer, K. Schwinghammer and B. V. Lotsch, *Chemical science*, 2014, **5**, 2789-2793.
8. X. Wang, L. Chen, S. Y. Chong, M. A. Little, Y. Wu, W.-H. Zhu, R. Clowes, Y. Yan, M. A. Zwijnenburg and R. S. Sprick, *Nature chemistry*, 2018, **10**, 1180-1189.
9. P. Pachfule, A. Acharjya, J. r. m. Roeser, T. Langenhahn, M. Schwarze, R. Schomäcker, A. Thomas and J. Schmidt, *Journal of the American Chemical Society*, 2018, **140**, 1423-1427.

10. S. Zhang, G. Cheng, L. Guo, N. Wang, B. Tan and S. Jin, *Angewandte Chemie*, 2020, **132**, 6063-6070.
11. C. B. Meier, R. Clowes, E. Berardo, K. E. Jelfs, M. A. Zwijnenburg, R. S. Sprick and A. I. Cooper, *Chemistry of Materials*, 2019, **31**, 8830-8838.
12. Z. Cheng, W. Fang, T. Zhao, S. Fang, J. Bi, S. Liang, L. Li, Y. Yu and L. Wu, *ACS applied materials & interfaces*, 2018, **10**, 41415-41421.
13. Y. Xu, N. Mao, C. Zhang, X. Wang, J. Zeng, Y. Chen, F. Wang and J.-X. Jiang, *Applied Catalysis B: Environmental*, 2018, **228**, 1-9.
14. R. S. Sprick, B. Bonillo, M. Sachs, R. Clowes, J. R. Durrant, D. J. Adams and A. I. Cooper, *Chemical Communications*, 2016, **52**, 10008-10011.
15. M. G. Schwab, M. Hamburger, X. Feng, J. Shu, H. W. Spiess, X. Wang, M. Antonietti and K. Müllen, *Chemical communications*, 2010, **46**, 8932-8934.
16. S. Ghosh, N. A. Kouamé, L. Ramos, S. Remita, A. Dazzi, A. Deniset-Besseau, P. Beaunier, F. Goubard, P.-H. Aubert and H. Remita, *Nature materials*, 2015, **14**, 505-511.
17. S. Ghosh, N. A. Kouame, S. Remita, L. Ramos, F. Goubard, P.-H. Aubert, A. Dazzi, A. Deniset-Besseau and H. Remita, *Scientific reports*, 2015, **5**, 1-9.
18. D. Floresyona, F. Goubard, P.-H. Aubert, I. Lampre, J. Mathurin, A. Dazzi, S. Ghosh, P. Beaunier, F. Brisset and S. Remita, *Applied Catalysis B: Environmental*, 2017, **209**, 23-32.
19. X. Yuan, D. Floresyona, P.-H. Aubert, T.-T. Bui, S. Remita, S. Ghosh, F. Brisset, F. Goubard and H. Remita, *Applied Catalysis B: Environmental*, 2019, **242**, 284-292.
20. L. Wu, J. Zheng, L. Wang, X. Xiong, Y. Shao, G. Wang, J. H. Wang, S. Zhong and M. Wu, *Angewandte Chemie*, 2019, **131**, 821-825.
21. M. Li, H. Li, W. Zhong, Q. Zhao and D. Wang, *ACS applied materials & interfaces*, 2014, **6**, 1313-1319.
22. H. Zarenezhad, T. Balkan, N. Solati, M. Halali, M. Askari and S. Kaya, *Solar Energy*, 2020, **207**, 1300-1307.
23. L. Zhang, Y. He, P. Luo, L. Ma, Y. Fan, S. Zhang, H. Shi, S. Li and Y. Nie, *Journal of Materials Chemistry A*, 2020, **8**, 4483-4493.
24. J. Pan, M. Yang, L. Luo, A. Xu, B. Tang, D. Cheng, G. Cai and X. Wang, *ACS applied materials & interfaces*, 2019, **11**, 7338-7348.
25. A. Angeli and L. Alessandri, *Gazz. Chim. Ital*, 1916, **46**, 279-285.

26. H. Shirakawa, E. J. Louis, A. G. MacDiarmid, C. K. Chiang and A. J. Heeger, *Journal of the Chemical Society, Chemical Communications*, 1977, 578-580.
27. C. K. Chiang, C. Fincher Jr, Y. W. Park, A. J. Heeger, H. Shirakawa, E. J. Louis, S. C. Gau and A. G. MacDiarmid, *Physical review letters*, 1977, **39**, 1098.
28. L. Dou, Y. Liu, Z. Hong, G. Li and Y. Yang, *Chemical reviews*, 2015, **115**, 12633-12665.
29. S. Lamprakopoulos, D. Yfantis, A. Yfantis, D. Schmeisser, J. Anastassopoulou and T. Theophanides, *Synthetic metals*, 2004, **144**, 229-234.
30. M. A. J. Mazumder, H. Sheardown and A. Al-Ahmed, *Functional Polymers*, Springer, 2019.
31. V. V. Tat'yana and O. N. Efimov, *Russian chemical reviews*, 1997, **66**, 443.
32. H. S. Nalwa, *Handbook of surfaces and interfaces of materials, five-volume set*, Elsevier, 2001.
33. R. Ansari, *Journal of Chemistry*, 2006, **3**, 186-201.
34. M. Satoh, K. Kaneto and K. Yoshino, *Synthetic metals*, 1986, **14**, 289-296.
35. J. Scott, J.-L. Bredas, K. Yakushi, P. Pfluger and G. Street, *Synthetic metals*, 1984, **9**, 165-172.
36. M. Ferenets and A. Harlin, *Thin solid films*, 2007, **515**, 5324-5328.
37. Y. Koo, B. Kim, D. Park and J. Joo, *Molecular Crystals and Liquid Crystals*, 2004, **425**, 55-60.
38. Q. Fang, D. Chetwynd and J. Gardner, *Sensors and Actuators A: Physical*, 2002, **99**, 74-77.
39. Z. Cui, C. Coletta, A. Dazzi, P. Lefrancois, M. Gervais, S. Néron and S. Remita, *Langmuir*, 2014, **30**, 14086-14094.
40. Y. Li, P. Bober, M. Trchová and J. Stejskal, *Journal of Materials Chemistry C*, 2017, **5**, 4236-4245.
41. D.-V. Brezoi, *Journal of Science and Arts*, 2010, **10**, 53.
42. E. Kang, K. Neoh, T. Matsuyama and H. Yamaoka, *Polymer communications Guildford*, 1988, **29**, 201-203.
43. E. Kang, H. Ti, K. Neoh and T. Tan, *Polymer journal*, 1988, **20**, 399-406.
44. S. Machida, S. Miyata and A. Techagumpuch, *Synthetic metals*, 1989, **31**, 311-318.
45. S. P. Armes, *Synthetic Metals*, 1987, **20**, 365-371.
46. S. Rapi, V. Bocchi and G. P. Gardini, *Synthetic Metals*, 1988, **24**, 217-221.
47. J. Y. Hong, H. Yoon and J. Jang, *Small*, 2010, **6**, 679-686.
48. Y. Liao, X.-G. Li and R. B. Kaner, *Acs Nano*, 2010, **4**, 5193-5202.
49. Y. Yang, Y. Chu, F. Yang and Y. Zhang, *Materials Chemistry and Physics*, 2005, **92**, 164-171.

50. J. Zhang, T. Qiu, S. Ren, H. Yuan, L. He and X. Li, *Materials Chemistry and Physics*, 2012, **134**, 1072-1078.
51. L. Hao, C. Zhu, C. Chen, P. Kang, Y. Hu, W. Fan and Z. Chen, *Synthetic metals*, 2003, **139**, 391-396.
52. S. M. Marinakos, J. P. Novak, L. C. Brousseau, A. B. House, E. M. Edeki, J. C. Feldhaus and D. L. Feldheim, *Journal of the American Chemical Society*, 1999, **121**, 8518-8522.
53. D. Cheng, H. Xia and H. S. O. Chan, *Langmuir*, 2004, **20**, 9909-9912.
54. K.-M. Mangold, J. Schuster and C. Weidlich, *Electrochimica Acta*, 2011, **56**, 3616-3619.
55. D. Su, J. Zhang, S. Dou and G. Wang, *Chemical Communications*, 2015, **51**, 16092-16095.
56. X. Liu, H. Wu, F. Ren, G. Qiu and M. Tang, *Materials Chemistry and Physics*, 2008, **109**, 5-9.
57. J. Zhao, J. Wu, B. Li, W. Du, Q. Huang, M. Zheng, H. Xue and H. Pang, *Progress in Natural Science: Materials International*, 2016, **26**, 237-242.
58. F.-L. Cheng, M.-L. Zhang and H. Wang, *Sensors*, 2005, **5**, 245-249.
59. J. Kopecká, D. Kopecký, M. Vrňata, P. Fitl, J. Stejskal, M. Trchová, P. Bober, Z. Morávková, J. Prokeš and I. Sapurina, *RSC Advances*, 2014, **4**, 1551-1558.
60. X. Zhang and S. K. Manohar, *Journal of the American Chemical Society*, 2005, **127**, 14156-14157.
61. X. Zhang and S. K. Manohar, *Journal of the American Chemical Society*, 2004, **126**, 12714-12715.
62. X. Yang, Z. Zhu, T. Dai and Y. Lu, *Macromolecular rapid communications*, 2005, **26**, 1736-1740.
63. Y. Yan, H. Li, Y. Zhang, J. Kan, T. Jiang, H. Pang, Z. Zhu and H. Xue, *Int. J. Electrochem. Sci.*, 2017, **12**, 9320-9334.
64. L. Yang, Z. Zhang, G. Nie, C. Wang and X. Lu, *Journal of Materials Chemistry A*, 2015, **3**, 83-86.
65. Z. Liu, X. Zhang, S. Poyraz, S. P. Surwade and S. K. Manohar, *Journal of the American Chemical Society*, 2010, **132**, 13158-13159.
66. J. Chen, D. Chao, X. Lu, W. Zhang and S. K. Manohar, *Macromolecular rapid communications*, 2006, **27**, 771-775.
67. L. M. Santino, S. Acharya and J. M. D'Arcy, *Journal of Materials Chemistry A*, 2017, **5**, 11772-11780.

68. C. Li, H. Bai and G. Shi, *Chemical Society Reviews*, 2009, **38**, 2397-2409.
69. E. Genies, G. Bidan and A. Diaz, *Journal of Electroanalytical Chemistry and Interfacial Electrochemistry*, 1983, **149**, 101-113.
70. K.-J. Kim, H.-S. Song, J.-D. Kim and J.-K. Chon, *Bulletin of the Korean Chemical Society*, 1988, **9**, 248-251.
71. S. Asavapiriyanont, G. Chandler, G. Gunawardena and D. Pletcher, *Journal of electroanalytical chemistry and interfacial electrochemistry*, 1984, **177**, 229-244.
72. Y. J. Qiu and J. R. Reynolds, *Journal of Polymer Science Part A: Polymer Chemistry*, 1992, **30**, 1315-1325.
73. S. Sadki, P. Schottland, N. Brodie and G. Sabouraud, *Chemical Society Reviews*, 2000, **29**, 283-293.
74. D.-H. Nam, M.-J. Kim, S.-J. Lim, I.-S. Song and H.-S. Kwon, *Journal of Materials Chemistry A*, 2013, **1**, 8061-8068.
75. J. Xing, S. Qi, Z. Wang, X. Yi, Z. Zhou, J. Chen, S. Huang, G. Tan, D. Chen and P. Yu, *Advanced Functional Materials*, 2019, 1806353.
76. J. M. Velazquez, A. V. Gaikwad, T. K. Rout, J. Rzayev and S. Banerjee, *ACS applied materials & interfaces*, 2011, **3**, 1238-1244.
77. Y. Chen, J. Meng, Z. Zhu, F. Zhang, L. Wang, Z. Gu, L. Jiang and S. Wang, *Advanced Functional Materials*, 2018, **28**, 1800240.
78. L. Qu, G. Shi, F. e. Chen and J. Zhang, *Macromolecules*, 2003, **36**, 1063-1067.
79. L. Qu, G. Shi, J. Yuan, G. Han and F. e. Chen, *Journal of Electroanalytical Chemistry*, 2004, **561**, 149-156.
80. L. Qu and G. Shi, *Journal of Polymer Science Part A: Polymer Chemistry*, 2004, **42**, 3170-3177.
81. Y. Gao, L. Zhao, C. Li and G. Shi, *Polymer*, 2006, **47**, 4953-4958.
82. Y. Gao, L. Zhao, H. Bai, Q. Chen and G. Shi, *Journal of Electroanalytical Chemistry*, 2006, **597**, 13-18.
83. H. Remita, I. Lampre, M. Mostafavi, E. Balanzat and S. Bouffard, *Radiation Physics and chemistry*, 2005, **72**, 575-586.
84. J. Belloni, M. Mostafavi, H. Remita, J.-L. Marignier and M.-O. Delcourt, *New Journal of Chemistry*, 1998, **22**, 1239-1255.

85. H. Remita and S. Remita, *Recent Trends in Radiation Chemistry. World Scientific Publishing Company, London*, 2010, 347-383.
86. J. F. Wishart and B. M. Rao, *Recent trends in radiation chemistry*, World Scientific, 2010.
87. J. W. T. Spinks and R. J. Woods, 1990.
88. C. Coletta, Z. Cui, P. Archirel, P. Pernot, J.-L. Marignier and S. Remita, *The Journal of Physical Chemistry B*, 2015, **119**, 5282-5298.
89. T. Bahry, Z. Cui, A. Deniset-Besseau, M. Gervais, C. Sollogoub, T.-T. Bui and S. Remita, *New Journal of Chemistry*, 2018, **42**, 8704-8716.
90. Z. Cui, C. Coletta, R. Rebois, S. Baiz, M. Gervais, F. Goubard, P.-H. Aubert, A. Dazzi and S. Remita, *Radiation Physics and Chemistry*, 2016, **119**, 157-166.
91. Z. Cui, T. Bahry, A. Dazzi, T.-T. Bui, F. Goubard and S. Remita, *Radiation Physics and Chemistry*, 2019, **159**, 47-56.
92. T. Bahry, Z. Cui, A. Deniset-Besseau, M. Gervais, I. Mbomekalle, C. Sollogoub, P.-H. Aubert, T.-T. Bui and S. Remita, *New Journal of Chemistry*, 2020, **44**, 11652-11666.
93. T. Bahry, B. Khurshid, Y. Chouli, S. Abou Zeid, C. Sollogoub, M. Gervais, T.-T. Bui, F. Goubard and S. Remita, *New Journal of Chemistry*, 2021, **45**, 13142-13157.
94. T. Bahry, Z. Cui, A. Dazzi, M. Gervais, C. Sollogoub, F. Goubard, T.-T. Bui and S. Remita, *Radiation Physics and Chemistry*, 2021, **180**, 109291.
95. Y. Chouli, F. Belkhadem-Mokhtari, S. Abou-Zeid, D. Dragoe, R. Saint-Martin, F. Briset, H. Remita and S. Remita, *Radiation Physics and Chemistry*, 2022, **Just accepted**.
96. J. Wang, J. Rong, Z. Fang, M. Wang, A. Asif, Q. Wu, X. Zhou and X. Ge, *Particle & Particle Systems Characterization*, 2017, **34**, 1600430.
97. J.-M. Kern and J.-P. Sauvage, *Journal of the Chemical Society, Chemical Communications*, 1989, 657-658.
98. C. Martins, Y. De Almeida, G. Do Nascimento and W. De Azevedo, *Journal of materials science*, 2006, **41**, 7413-7418.
99. X. Yang and Y. Lu, *Materials letters*, 2005, **59**, 2484-2487.
100. K. M. Coakley and M. D. McGehee, *Chemistry of materials*, 2004, **16**, 4533-4542.
101. X. Yuan, D. Dragoe, P. Beaunier, D. B. Uribe, L. Ramos, M. G. Méndez-Medrano and H. Remita, *Journal of Materials Chemistry A*, 2020, **8**, 268-277.

102. J. Low, J. Yu, M. Jaroniec, S. Wageh and A. A. Al-Ghamdi, *Advanced materials*, 2017, **29**, 1601694.
103. W. Lee, D. Kim, S. Lee, J. Park, S. Oh, G. Kim, J. Lim and J. Kim, *Nano Today*, 2018, **23**, 97-123.
104. S. Li, M. Chen, L. He, F. Xu and G. Zhao, *Journal of Materials Research*, 2009, **24**, 2547-2554.
105. L. Sun, Y. Shi, B. Li, X. Li and Y. Wang, *Polymer Composites*, 2013, **34**, 1076-1080.
106. D. Chowdhury, A. Paul and A. Chattopadhyay, *Langmuir*, 2005, **21**, 4123-4128.
107. F. Deng, Y. Li, X. Luo, L. Yang and X. Tu, *Colloids and Surfaces A: Physicochemical and Engineering Aspects*, 2012, **395**, 183-189.
108. S. Ghosh, L. Ramos and H. Remita, *Nanoscale*, 2018, **10**, 5793-5819.
109. X. Yuan, M. P. Kobylanski, Z. Cui, J. Li, P. Beaunier, D. Dragoe, C. Colbeau-Justin, A. Zaleska-Medynska and H. Remita, *Journal of Environmental Chemical Engineering*, 2020, **8**, 104178.
110. S. Li, S. Xu, L. He, F. Xu, Y. Wang and L. Zhang, *Polymer-plastics technology and engineering*, 2010, **49**, 400-406.
111. L. Zhou, W. Wang, H. Xu, S. Sun and M. Shang, *Chemistry–A European Journal*, 2009, **15**, 1776-1782.
112. F. Amano, A. Yamakata, K. Nogami, M. Osawa and B. Ohtani, *Journal of the American Chemical Society*, 2008, **130**, 17650-17651.
113. R. Li, F. Zhang, D. Wang, J. Yang, M. Li, J. Zhu, X. Zhou, H. Han and C. Li, *Nature communications*, 2013, **4**, 1-7.
114. H. Cheng, B. Huang, K. Yang, Z. Wang, X. Qin, X. Zhang and Y. Dai, *ChemPhysChem*, 2010, **11**, 2167-2173.
115. D. Sánchez-Rodríguez, M. G. M. Medrano, H. Remita and V. Escobar-Barrios, *Journal of environmental chemical engineering*, 2018, **6**, 1601-1612.
116. Z. Zhao, Y. Cao, F. Dong, F. Wu, B. Li, Q. Zhang and Y. Zhou, *Nanoscale*, 2019, **11**, 6360-6367.
117. X. Liu and L. Cai, *Applied Surface Science*, 2018, **445**, 242-254.
118. J. Xu, Y. Hu, C. Zeng, Y. Zhang and H. Huang, *Journal of colloid and interface science*, 2017, **505**, 719-727.
119. F. Duan, Q. Zhang, D. Shi and M. Chen, *Applied Surface Science*, 2013, **268**, 129-135.

120. Q. Wang, L. Zheng, Y. Chen, J. Fan, H. Huang and B. Su, *Journal of Alloys and Compounds*, 2015, **637**, 127-132.
121. B. Yan, Y. Wang, X. Jiang, K. Liu and L. Guo, *ACS applied materials & interfaces*, 2017, **9**, 29113-29119.
122. F. A. Harraz, A. A. Ismail, S. Al-Sayari and A. Al-Hajry, *Journal of Photochemistry and Photobiology A: Chemistry*, 2015, **299**, 18-24.
123. R. Gogoi, A. Singh, V. Moutam, L. Sharma, K. Sharma, A. Halder and P. F. Siril, *Journal of Environmental Chemical Engineering*, 2022, **10**, 106649.
124. D. Wang, Y. Xu, M. Xie, Y. Song, H. Xu, H. Li and J. Xie, *Journal of hazardous materials*, 2019, 121480.
125. M. Abinaya, R. Rajakumaran, S.-M. Chen, R. Karthik and V. Muthuraj, *ACS applied materials & interfaces*, 2019, **11**, 38321-38335.
126. L. Midya, A. Chettri and S. Pal, *ACS Sustainable Chemistry & Engineering*, 2019, **7**, 9416-9421.
127. Y. Zhang, J. Liu, S.-L. Li, Z.-M. Su and Y.-Q. Lan, *EnergyChem*, 2019, 100021.
128. X. Xu, X. Gao, Z. Cui, X. Liu and X. Zhang, *Dalton transactions*, 2014, **43**, 13424-13433.
129. Y. Yang, J. Wen, J. Wei, R. Xiong, J. Shi and C. Pan, *ACS applied materials & interfaces*, 2013, **5**, 6201-6207.
130. D. Hao, Y. Yang, B. Xu and Z. Cai, *ACS Sustainable Chemistry & Engineering*, 2018, **6**, 10789-10797.
131. F. Deng, L. Min, X. Luo, S. Wu and S. Luo, *Nanoscale*, 2013, **5**, 8703-8710.
132. L. Cai, H. Jiang and L. Wang, *Applied Surface Science*, 2017, **420**, 43-52.
133. Y. Lin, X. Wu, Y. Han, C. Yang, Y. Ma, C. Du, Q. Teng, H. Liu and Y. Zhong, *Applied Catalysis B: Environmental*, 2019, **258**, 117969.
134. S. Ghosh, D. Rashmi, S. Bera and R. N. Basu, *International Journal of Hydrogen Energy*, 2019, **44**, 13262-13272.
135. M. Janczarek and E. Kowalska, *Catalysts*, 2017, **7**, 317.
136. S. Ghosh, S. R. Keshri, S. Bera and R. N. Basu, *International Journal of Hydrogen Energy*, 2020, **45**, 6159-6173.
137. T. A. Kandiel, R. Dillert and D. W. Bahnemann, *Photochemical & Photobiological Sciences*, 2009, **8**, 683-690.

138. N. M. Dimitrijevic, S. Tepavcevic, Y. Liu, T. Rajh, S. C. Silver and D. M. Tiede, *The Journal of Physical Chemistry C*, 2013, **117**, 15540-15544.
139. X. Li, P. Wang, B. Huang, X. Qin, X. Zhang, Q. Zhang, X. Zhu and Y. Dai, *International Journal of Hydrogen Energy*, 2017, **42**, 25195-25202.
140. M. Sathish and R. Viswanath, *Catalysis Today*, 2007, **129**, 421-427.
141. S. Zhang, Q. Chen, Y. Wang and L. Guo, *international journal of hydrogen energy*, 2012, **37**, 13030-13036.
142. X. Wang, K. Maeda, A. Thomas, K. Takanabe, G. Xin, J. M. Carlsson, K. Domen and M. Antonietti, *Nature materials*, 2009, **8**, 76.
143. Y. Sui, J. Liu, Y. Zhang, X. Tian and W. Chen, *Nanoscale*, 2013, **5**, 9150-9155.
144. X. Yuan, C. Wang, D. Dragoe, P. Beaunier, C. Colbeau-Justin and H. Remita, *Applied Catalysis B: Environmental*, **281**, 119457.
145. N. Kumar, S. Kumar, R. Gusain, N. Manyala, S. Eslava and S. S. Ray, *ACS Applied Energy Materials*, 2020, **3**, 9897-9909.
146. F. Kuttassery, H. Kumagai, R. Kamata, Y. Ebato, M. Higashi, H. Suzuki, R. Abe and O. Ishitani, *Chemical science*, 2021, **12**, 13216-13232.
147. X. Yuan, université Paris-Saclay, 2020.
148. R. Nosrati, A. Olad and F. Maryami, *Journal of Molecular Structure*, 2018, **1163**, 174-184.
149. L. Děkanovský, R. Elashnikov, M. Kubiková, B. Vokatá, V. Švorčík and O. Lyutakov, *Advanced Functional Materials*, 2019, **29**, 1901880.
150. X. Yuan, Q. Mu, S. Xue, Y. Su, Y. Zhu, H. Sun, Z. Deng and Y. Peng, *Journal of Energy Chemistry*, 2021, **60**, 202-208.
151. X. Peng, J. Li, L. Yi, X. Liu, J. Chen, P. Cai and Z. Wen, *Applied Catalysis B: Environmental*, 2022, **300**, 120737.
152. H. Mao, Y. Fu, H. Yang, Z.-z. Deng, Y. Sun, D. Liu, Q. Wu, T. Ma and X.-M. Song, *ACS applied materials & interfaces*, 2020, **12**, 25189-25199.